MCR-76-564

Contract NAS2-9381

(NASA-CR-152123-Task-2-Final) INFRARED IMAGERY OF SHUTTLE (IRIS). TASK 2 Final Report (Martin Marietta Corp.) 58 p HC A04/MF A01

CSCL 22B

N81-25133

Unclas G3/16 26039

Task 2

Final Report

January 1978

Infrared Imagery of Shuttle (IRIS)

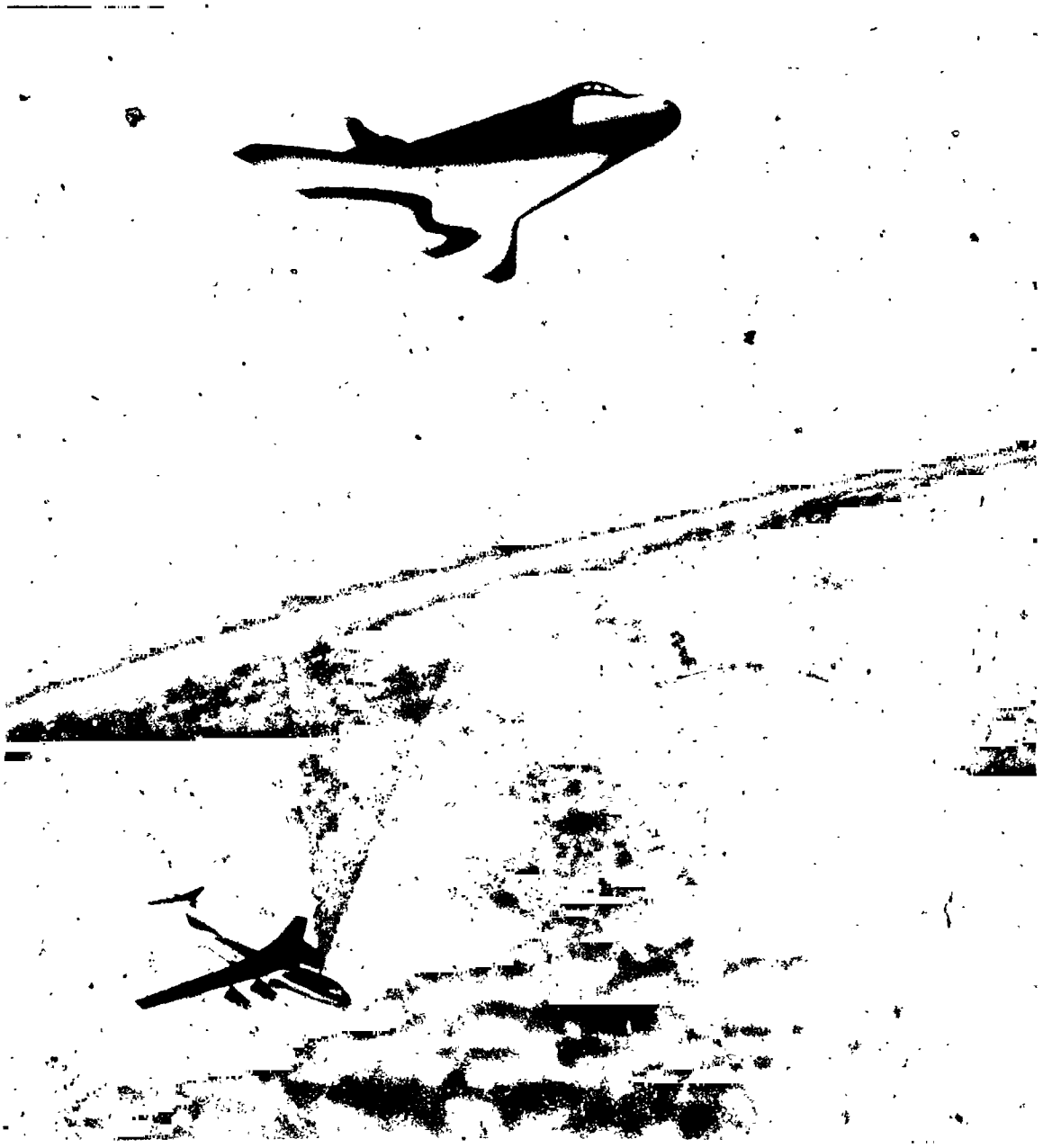

MARTIN MARIETTA

MCR-76-564

Contract NAS2-9381

Final
Report

January 1978

Task 2

INFRARED IMAGERY OF SHUTTLE (IRIS)

Approved

Clifford J. Chocol
Program Manager

MARTIN MARIETTA CORPORATION
P. O. Box 179
Denver, Colorado 80201

CONTENTS

Figure

SUMMARY

Based on key breadboard tests of specific portions of the design, it has been established that the Infrared Imagery of Shuttle (IRIS) program is practical and will provide the Shuttle entry temperature information required to evaluate Shuttle surface heating*. The measurements are not easy, and extreme care will be required at every step of design, installation, checkout, and calibration of the flight system to obtain the desired result.

End-to-end tests of a 16 element indium antimonide sensor array and 10 channels of associated electronic signal processing have been completed. Quantitative data have been gathered on system responsivity, frequency response, noise, stray capacitance effects, and sensor paralleling. These tests verify that the temperature accuracies, predicted in the Task 1 study, can be obtained with a very carefully designed electro-optical flight system. Pre-flight and inflight calibration of a high quality are mandatory to obtain these accuracies. Also, optical crosstalk in the array-dewar assembly must be carefully eliminated by its design.

Tests of the scaled up tracking system reticle also demonstrate that the tracking system accuracies predicted in the Task 1 study can be met in the flight system. In addition, improvements in the reticle pattern and electronics are possible, which will reduce the complexity of the flight system and increase tracking accuracy.

*This report is an addendum to Martin Marietta Corporation Report MCR-76-564 entitled *Infrared Imagery of Shuttle (IRIS) - Task 1*, where details of the experiment concept and equipment design can be found.

INTRODUCTION

The purpose of the Task 2 effort was to produce an opto-electronic breadboard of 10 channels of the IR temperature measuring system and a scaled up portion of the tracking system reticle. The purpose of these two breadboards was to allow testing that would verify assumptions made in Task 1 or to provide data that simply did not exist in Task 1. This report contains a description of the breadboards and the tests performed on them. The raw data, reduced data, and conclusions to be reached from each significant test are contained in this report. Conclusions appear at the end of the Chapter I, Imaging System, and again at the end of Chapter II, Acquisition System Analysis and Test.

I. IMAGING SYSTEM

A. ELECTRONIC TESTS

This section contains the results of testing of the Imaging Electronics Breadboard shown schematically in Figure 1(a). All testing was electrical and was pointed toward understanding the data system transfer function from simulated IR detector input to the DATEL DAS 250 digital output. The transfer function was tested for innate characteristics of certain hardware elements such as the DAS 250 and for parameters that could be controlled in the design such as amplifier input capacitance. Figure 1(b) is a photograph of the laboratory setup.

1. Imaging Electronics Breadboard Description

Figure 1(a) shows the signal paths through the calibration resistors, into the trans-resistance amplifiers, through the active low pass filters, and into the DAS 250 data system. The DAS 250 is a 16-channel commercial data system built by Datel Corporation. It contains a high-level multiplexer, a high-speed sample and hold and a 12-bit analog-to-digital converter. The input to the multiplexer is available as ±5 V or 0 to -10 V. The 0- to -10-V version was used in the breadboard. The DAS 250 was used in a sequential mode in which the multiplexer advances one channel each time an external convert pulse is applied to the hardware. The channel number at which the multiplexer resets back to Channel 1 is programmable by patching on the breadboard. Tests were run with only Channel 1 or Channels 1, 2, and 3 or Channels 1 through 10 being multiplexed.

All testing was performed using a parallel digital data output. The 12-bit outputs were taken into a Tektronix 7904 oscilloscope with a 7D01 logic analyzer. Data were taken two ways. Most of the raw data contained in this report are photographs of the CRT. Data displayed on the CRT were usually rows of 16-bit binary numbers. The right-hand 12 bits are always the output of the DAS 250 and represent the conversion of a single analog measurement. The most significant bit is on the left (see Fig. 10). Occasionally the data are displayed in the form of a timing diagram. In thatform, the top line in the photograph represents the least significant bit as a function of time; the 12th line represents the most significant bit. The reason for including this type of data is that more than 1000 bits of information can be shown in one photograph. These photographs were usually taken to show the digital noise level over many samples (see Fig. 5).

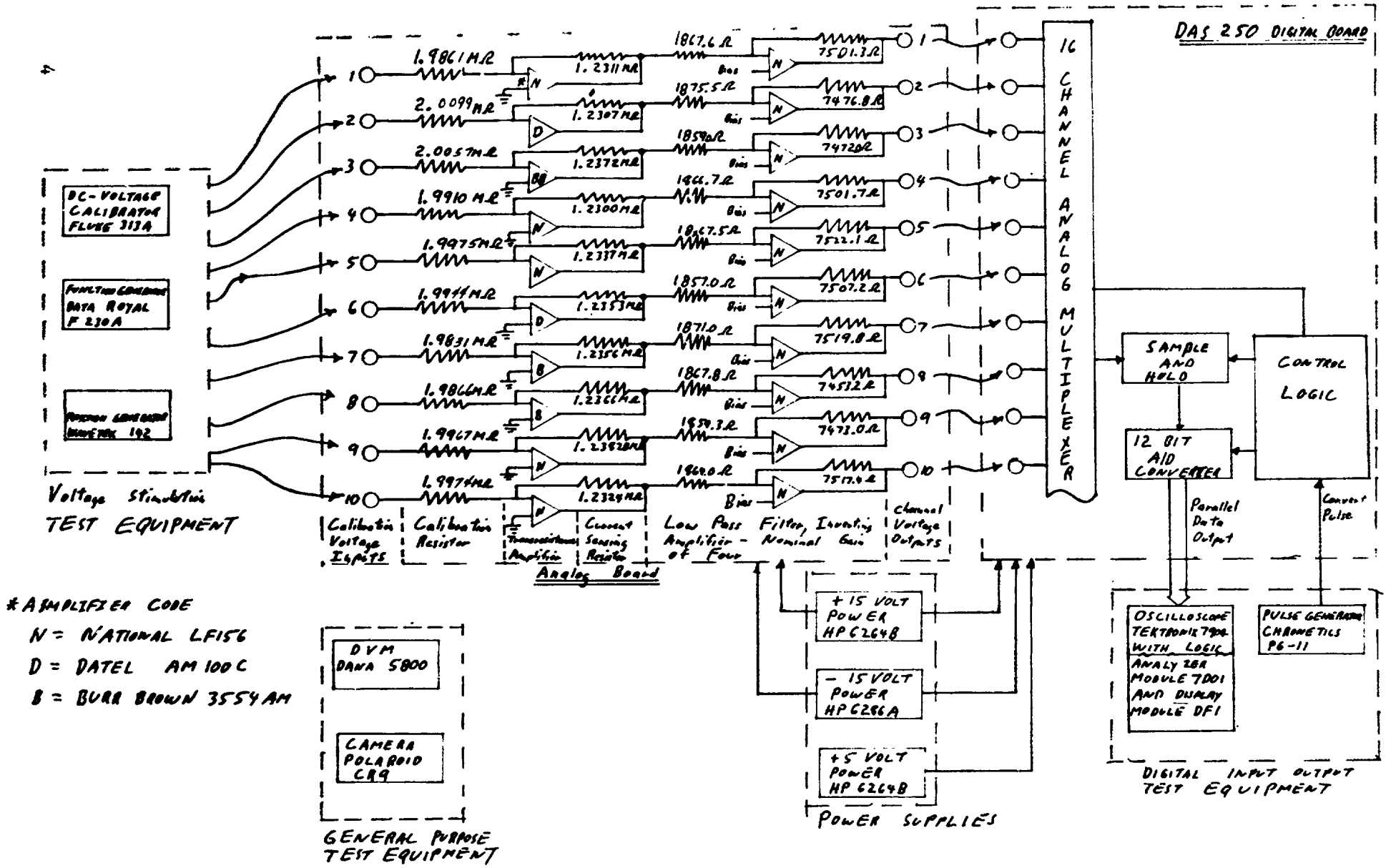

*AMPLIFIER CODE

N = NATIONAL LF156

D = DATEL AM 100 C

B = BURR BROWN 3554 AM

Figure 1(a) Data System Electronic and Test - Block Diagram

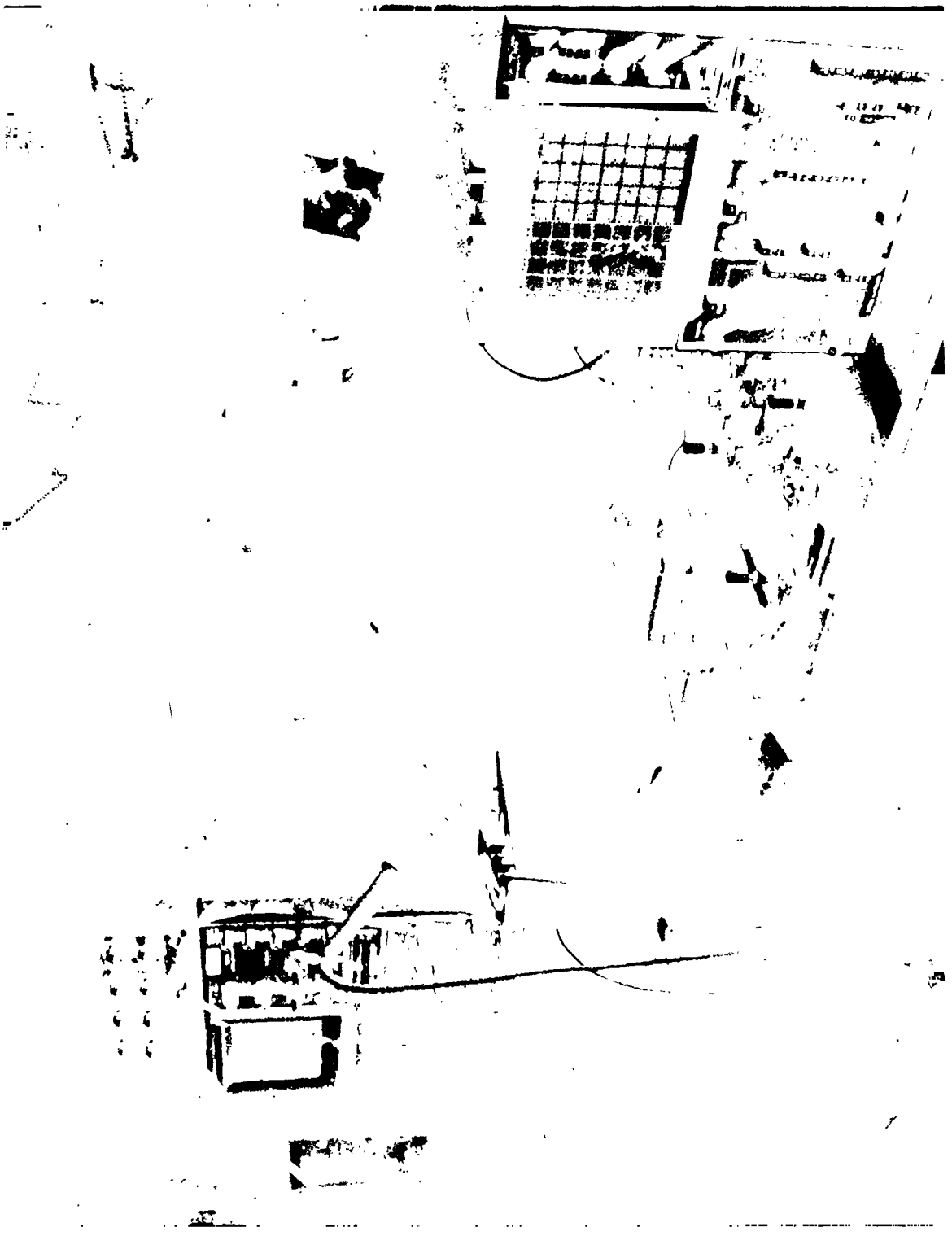

Figure 1(b) Laboratory Setup

Another feature of the breadboard that must be clearly understood to interpret the test data is the use of calibration resistors to simulate IR sensor current. In Figure 1(a) it is apparent that the current that will flow through a calibration resistor is equal to the input calibration or function generator voltage minus the amplifier input voltage divided by the size of the calibration resistor. This is valid only because the amplifiers maintain a near perfect virtual ground on the signal input.

Three kinds of wide bandwidth amplifiers were selected for evaluation in the breadboard. Figure 2 is a summary of the amplifier characteristics. Figure 1(a) identifies the amplifier type used in each channel.

2. Electrical Noise

Figure 3, 4, and 5 show the transresistance amplifier output noise with very low input capacitance, a few picofarads per channel and with the inputs open circuited. Noise will increase as input capacitance increases, but in this test all channels show a noise level of only one least significant bit (LSB). Two conclusions are reached. The amplifiers will support the use of a 12-bit data system and all three types of amplifiers are satisfactory, considering only this test.

3. DC Offset

With the inputs open to all channels, the offset voltages were measured on the transresistance amplifier outputs and the low pass filter outputs.

The low pass filter output is due to the bias voltage for the low pass filter amplifier. Because of the negative voltage output from the transresistance amplifier, the inverting nature of the active filter amplifier and the 0- to -10-V range of the DAS 250 it was necessary to put a nominal -10-V range bias on this amplifier. That bias is shown in Figure 6.

The transresistance amplifiers are all referenced to circuit ground and the offsets shown in Figure 6 are due entirely to the amplifier for Channels 1, 5, 9 and 10. All other channels contained a zero offset adjustment. Unfortunately, Channels 3 and 7 were not properly adjusted when the data were taken. Referring back to the input offset voltages listed in Figure 2 for the three amplifier types and considering the measured output offset voltages in Figure 6, it is concluded that offset voltage has not affected the virtual ground at the amplifier input.

TYPE	OPEN LOOP GAIN	GAIN BANDWIDTH PRODUCT	SETTLING TIME TO .01%	FULL POWER RESPONSE	SLEW RATE	INPUT RESISTANCE	INPUT NOISE VOLTAGE	INPUT OFF SET VOLTAGE	INPUT OFF SET CURRENT
NATIONAL 156		5 MHz	1.4 us		15v/us		$\frac{12nv}{\sqrt{Hz}}$	3 mv	30 pa
DATEL AM100C	500,000	18 MHz	.4 us	900 KHz	60v/us	10^{12}	$\frac{25nv}{\sqrt{Hz}}$	Adjust-able to zero	$\pm$ 10 pa
BURR BROWN 3554 AM	100,000	225 to 1700 MHz depending on compensa-tion	.2 us	19 MHz	1200v/us	10"	7 to $\frac{125nv}{\sqrt{Hz}}$	$\pm\frac{1}{2}$ mv	-10 pa

Figure 2 - Summary of Operational Amplifier Characteristics

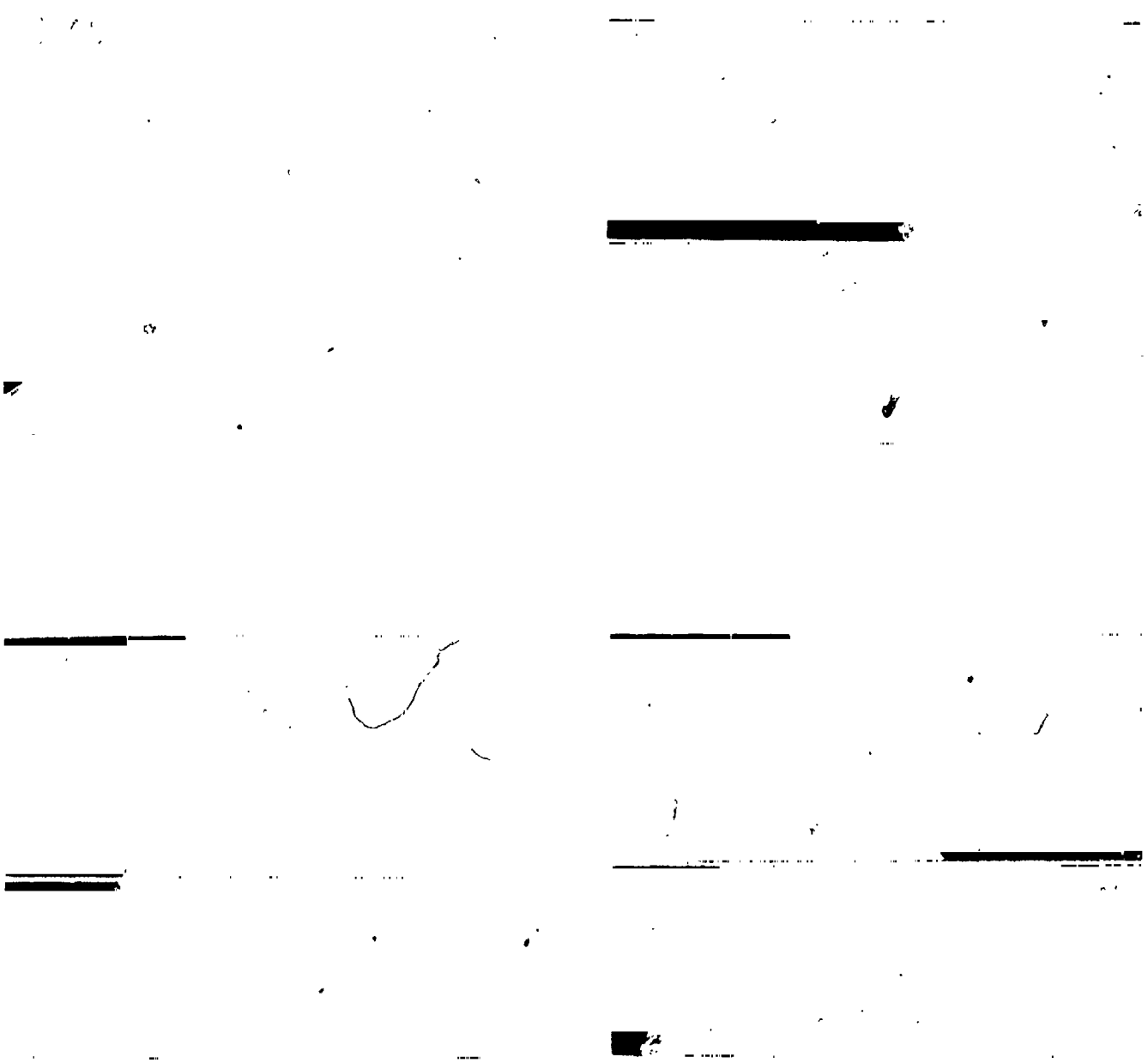

Channel 2 Output

Channel 3 Output

Note all Pictures are 20mv and 100us/CM

Figure 3 - Quiescient Noise Channel 1, 2, and 3 Outputs

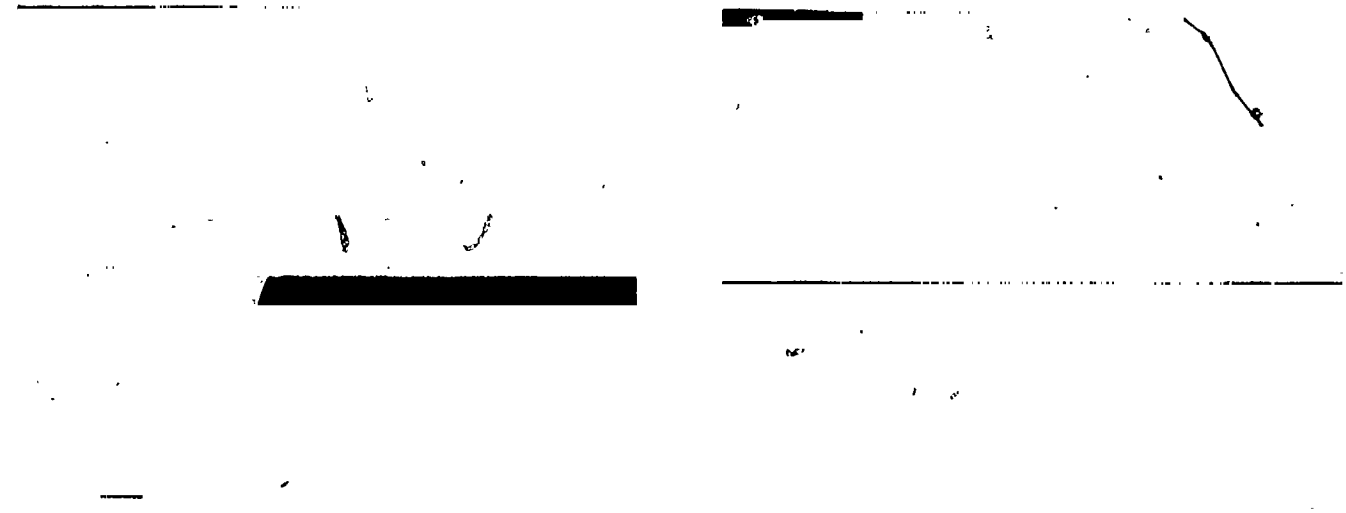

Channel 2 Unfiltered

Note - All pictures 20mv, 100us/CM

Channel 3 Unfiltered

Figure 4 - Quiescient Noise, Transresistance Amplifier Outputs

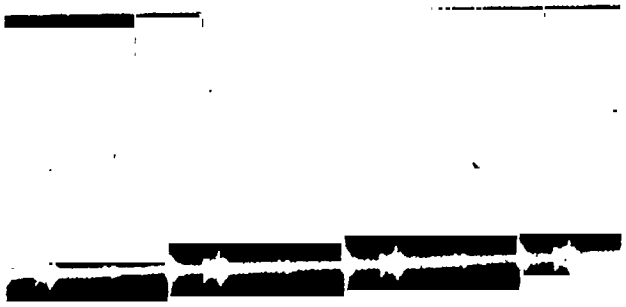

Channel 1 Output with DAS 250
Running 20mv, 2us/CM

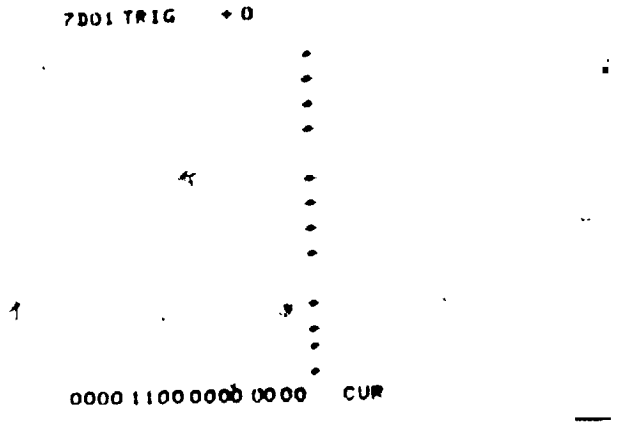

Channel #1 Digital Output LSB at Top and
MSB at Bottom

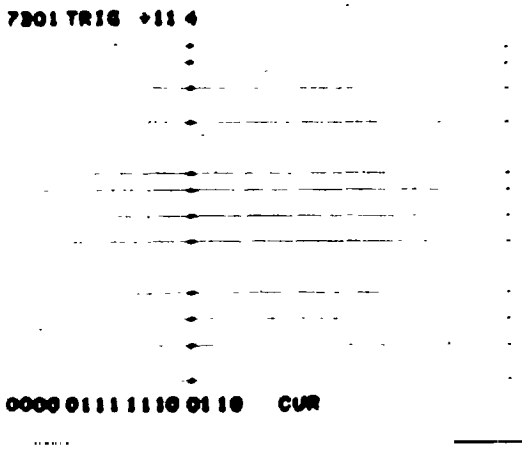

Channel 2 Digital Output

Channel 3 Digital Output

**Figure 5 - Analog and Digital Outputs with DAS 250
Running at 200,000 Conversions per Second**

TRANSRESISTANCE		LO PASS
CHANNEL	AMPLIFIER OUTPUT	FILTER OUTPUT
1	+ .0002	- 9.989
2	+ .0109	- 9.9945
3	+ .305	- 9.9952
4	Failed Amplifier (Unit replaced in later testing)	
5	+ .0022	- 9.9940
6	+ .006	- 9.9934
7	+ .48	- 9.9948
8	+ .01	- 9.993
9	+ .0036	- 9.994
10	+ .001	- 9.988

Figure 6 - DC Offset Measurements

4. DC Gain

Figure 7 relates the dc voltage applied to the calibration resistor, calculated current flowing into the transresistance amplifier summing junction, and then to output counts of the DAS 250. In the final design, careful attention must be given to the affects of the offset voltages on this calibration current. For purposes of this report, the summing junction of each transresistance amplifier is assumed to be exactly at ground potential.

To increase the confidence that the calibration currents listed in Figure 7 are accurate, Figure 8 compares the transfer function of the DAS 250 under two conditions. In Figure 8, the measured transfer function is the mv/count for the DAS 250. The data are best understood by recognizing that the calibration voltages on each channel were adjusted to produce an output of 4094 counts (about 10 V). That voltage then divided by the delta counts (4093) produced the 2.4408 mv/count number listed in Figure 8. The "calculated transfer function" shown in Figure 8 was produced by calculating each channel voltage output using the calibration current from Figure 7 and the circuit gains implicit in Figure 1(a). That voltage was then scaled to mv/count and compared to the measured value.

If the two sets of numbers agree, it means the simulation of IR detector current in these circuits is accurate. From Figure 8 it is seen that the best channel agrees to within 0.02% and the worst is off by 0.2%. The average difference between the measured and calculated transfer functions is 0.07%. The conclusion is that the calibration approach is valid and supports the measurement accuracies desired in this system. The 0.2% difference in the Channel 2 DATEL transfer functions should be understood if the DATEL amplifier is considered in the flight design.

5. Sine Wave Gain

Only Channel 1 was tested. Using a four-place Fluke DVM as an ac voltmeter, the 3 dB rolloff point is found at 47 kHz. At 18 kHz, the response is down 0.9%. The response appears to be quite flat to 10,000 Hz. Figure 9 shows the sine wave response at these frequencies. The corresponding ac calibration voltage gain is shown in Figure 9(a).

6. Ramp Test 1 (Maximum Rate)

Three multiplexer channels were programmed for a combined sample rate of 250,000 samples a second. A fixed synchronization word was generated by one channel. The other two channels monitored the input and the output of analog Channel 1. Figure 10 shows the output ramp function and the digital data recorded by the logic analyzer. Table I represents the input and output slopes reduced from the digital data. The rise time on the channel output was 10 V in 25 μs.

CHANNEL	CALIBRATION VOLTAGE	CALCULATED CALIBRATION CURRENT u amps	DAS 250 OUTPUT DIGITAL COUNTS	AMPERES/ COUNT
1	0	0	0	$4,935 \times 10^{-10}$
	4.0130	2.021	4094	
2	0	0	1	4.987×10^{-10}
	4.1040	2.042	4094	
3	0	0	1	4.9104×10^{-10}
	4.0311	2.010	4094	
4	Failed Channel			
5	0	0	1	4.913×10^{-10}
	4.0167	2.011	4094	
6	0	0	2	4.8915×10^{-10}
	3.992	2.002	4094	
7	0	0	1	4.9291×10^{-10}
	3.996	2.015	4094	
8	0	0	1	4.9476×10^{-10}
	4.023	2.025	4094	
9	0	0	1	4.9197×10^{-10}
	4.0157	2.011	4094	
10	0	0	1	4.9147×10^{-10}
	4.017	2.011	4094	

Figure 7 Calibration Voltage to DAS 250 Transfer Function, at DC (DC Gain)

CHANNEL NUMBER	INPUT AMPLIFIER TYPE	MEASURED TRANSFER FUNCTION/ mv/count	CALCULATED TRANSFER FUNCTION mv/count	% DIFFERENCE
1	N	2.4408	2.4392	.07
2	D	2.4408	2.4458	.20
3	B	2.4408	2.4400	.03
4	N	Failed Channel		
5	N	2.4408	2.4396	.05
6	D	2.4408	2.4404	.02
7	B	2.4408	2.4430	.09
8	B	2.4408	2.4396	.05
9	N	2.4408	2.4437	.12
10	N	2.4408	2.4403	.02

Figure 8 - Measured Versus Calculated DC Transfer Function

FREQUENCY HZ/SEC	MEASURED VOLTAGE GAIN	% DIFFERENCE
DC	2.4858	0
100	2.4859	+ .004
1,000	2.4836	- .080
10,000	2.4850	- .032
18,000	2.4641	- .873
47,000	2.0151	-30.000

Figure 9(a) Channel 1 Gain Versus Frequency

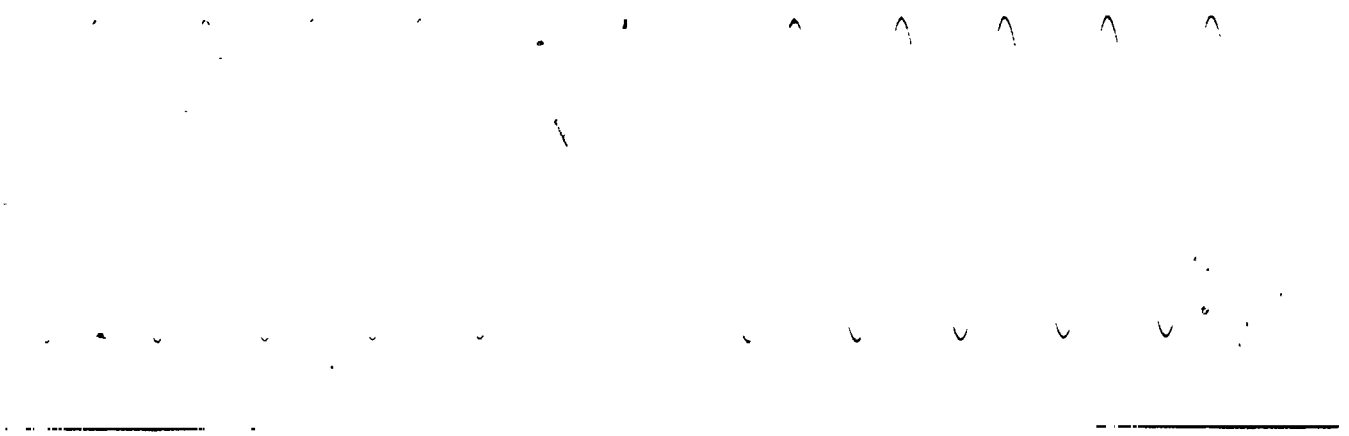

1000 Hz

10,000 Hz

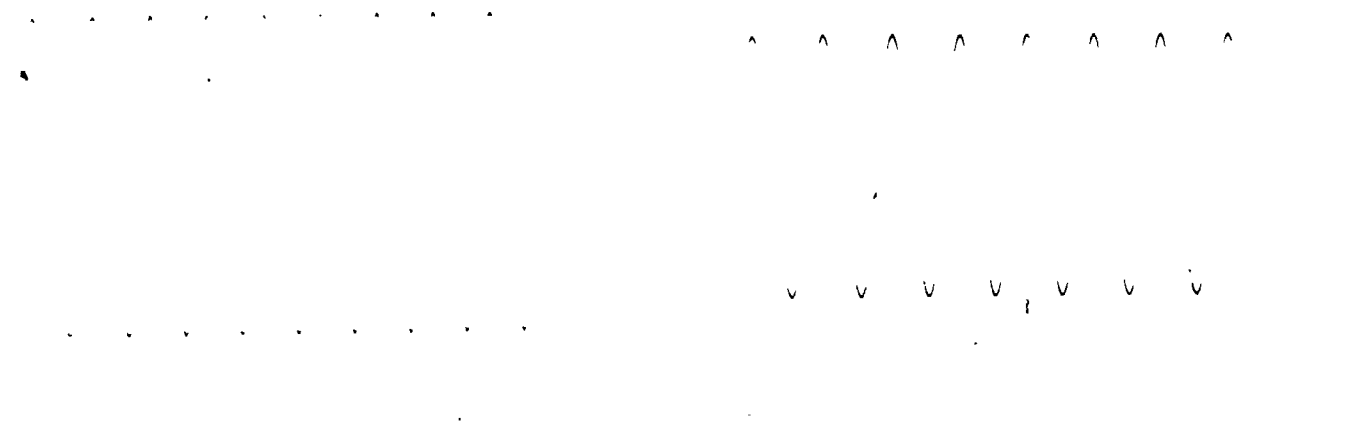

18000 Hz

47,000 Hz

Note - All Pictures are 1 volt/CM

Figure 9 - Channel #1 Sine Wave Response

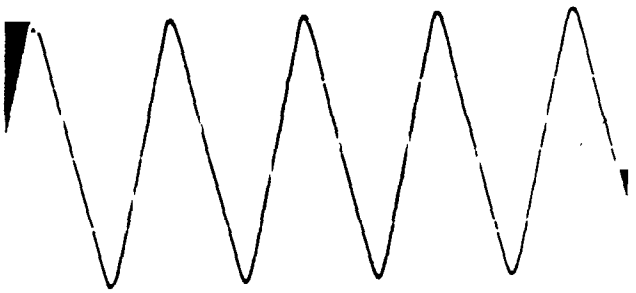

Output Ramp 50 us/CM 5v/CM

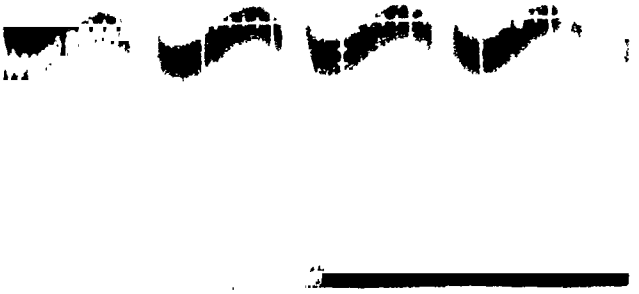

Noise on Channel 1 Output with DAS 250
Running 1mv/CM 2us/CM

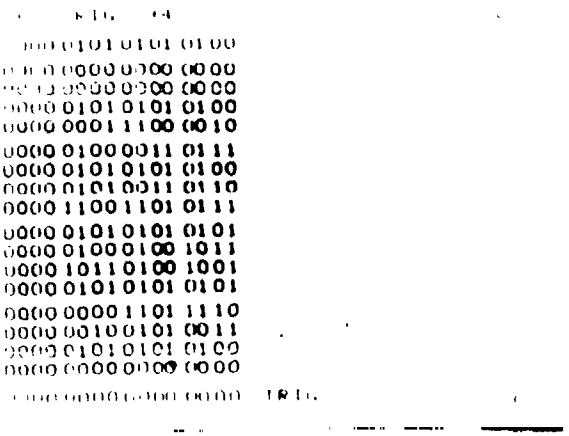

Digital Data Plotted in Table

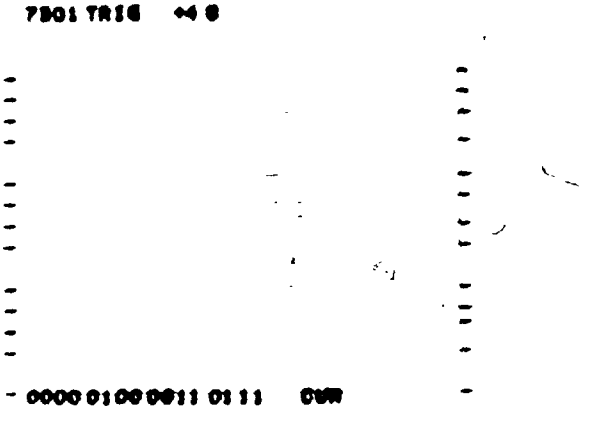

48 Samples of Ramp Data

Figure 10 Ramp Test #1

TABLE I

RAW DATA	INPUT COUNTS	OUTPUT COUNTS	INPUT SLOPE	INPUT SLOPE X DC GAIN	OUTPUT SLOPE	% DIFFERENCE
0001 1100 0010	450					
0100 0011 0111		1079	884	2197		
0101 0011 0110	1334					
1100 1101 0111		3287			2208	.5
0100 0100 1011	1099					
1011 0100 1001		2889				
0000 1101 1110	222		877	2180		
0010 0101 0011		595			2294	5

This test is equivalent to attempting to measure a function with twice the slope of the leading edge of the Shuttle image. Clearly, that is not a requirement in the flight system. No further effort was expended to clarify the 5% error.

7. Ramp Test 2

In this ramp test, the second amplifier was biased as it would be in the flight system, so that a zero to plus full-scale signal would be encoded as a -10 V to zero signal. Figure 11 shows the input and output of Channel 1 with a triangular wave that simulates the rise time of the Shuttle leading edge, 10 V in 50 μs. Figures 12 and 13 contain the analog wave form pictures and the raw data. A comparison of input and output slopes, with the input slope multiplied by the dc gain function is contained in Table II. The slope agreement is 2½%.

TABLE II

SAMPLE NUMBERS	INPUT SLOPE	INPUT SLOPE X DC GAIN	OUTPUT SLOPE	% DIFFERENCE
15 & 18	417	1037		
				2.4%
10 & 13			1062	
33 & 36	433	1076		
				2.1%
40 & 43			1099	

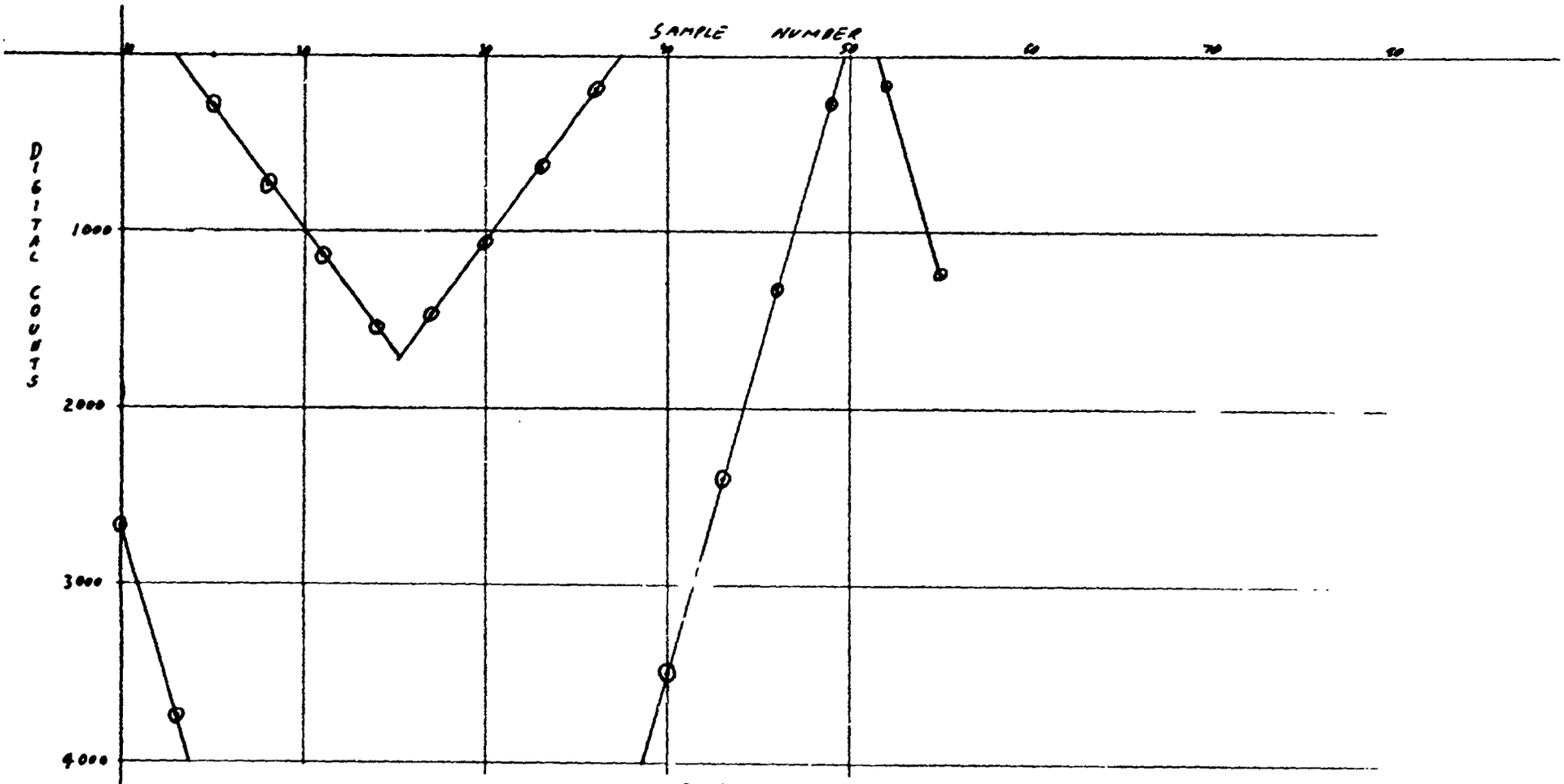

Sample #

Channel #1

Sample #				Counts	Check
9	0 0 0 0	0 0 0 0	0 0 0 0	0 0 0 0	
12	0 0 0 0	0 0 0 0	0 0 0 0	0 0 0 0	
15	0 0 0 1	0 0 1 0	1 0 0 0	0 2 9 6	417
18	0 0 1 0	1 1 0 0	1 0 0 1	0 7 1 3	409
21	0 1 0 0	0 1 1 0	0 0 1 0	1 1 2 2	398
24	0 1 0 1	1 1 1 1	0 0 0 0	1 5 2 0	398
27	0 1 0 1	1 0 1 1	1 0 1 0	1 9 6 0	411
30	0 1 0 0	0 0 0 1	1 1 1 1	1 0 5 5	425
33	0 0 1 0	0 1 1 1	0 1 1 0	6 3 0	433
36	0 0 0 0	1 1 0 0	0 1 0 1	1 9 7	
39	0 0 0 0	0 0 0 0	0 0 0 0	0 0 0 0	
42					
45					
48					
51					
54					
57					

Channel #2

				Counts	Check
10	1 0 1 0	0 1 1 1	1 0 1 0	2 6 8 2	1062
13	1 1 1 0	1 0 1 0	0 0 0 0	3 7 9 4	
16	1 1 1 1	1 1 1 1	1 1 1 1		
19	1 1 1 1	1 1 1 1	1 1 1 1		
22					
25					
28					
31					
34					
37	1 1 1 1	1 1 1 1	1 1 1 1		
40	1 1 0 1	1 0 1 0	1 1 0 0	3 5 0 0	1099
43	1 0 0 1	0 1 1 0	0 0 0 1	2 9 0 1	1084
46	0 1 0 1	0 0 1 0	0 1 0 1	1 3 1 7	1059
49	0 0 0 1	0 0 0 0	0 0 1 0	2 5 8	
52	0 0 0 0	1 0 0 1	1 1 1 1	1 5 9	1074
55	0 1 0 0	1 1 0 1	0 0 0 1	1 2 3 3	

Figure 11
Ramp Test #2

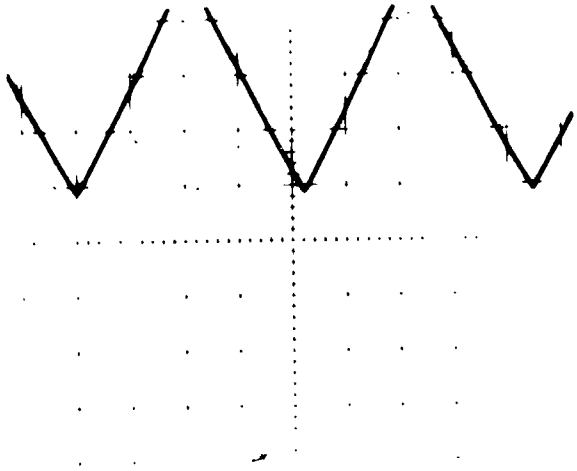

Channel #1 Input 2v and 50us/CM
Ground is 1 CM from Top Frequenc
= 4500 Hz

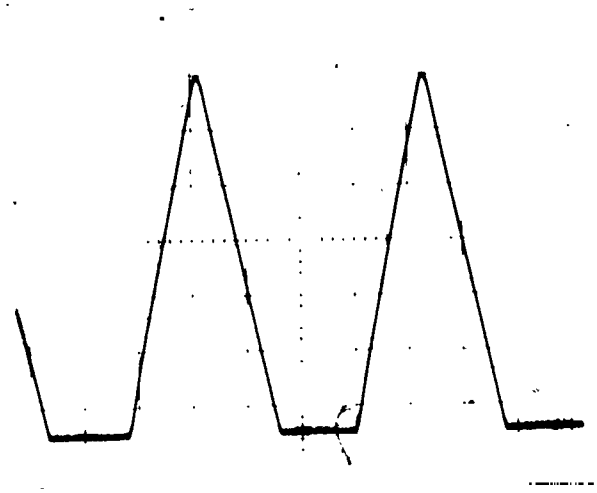

Channel #1 Output 2v and 50us/CM
Ground is 1 CM from the Top

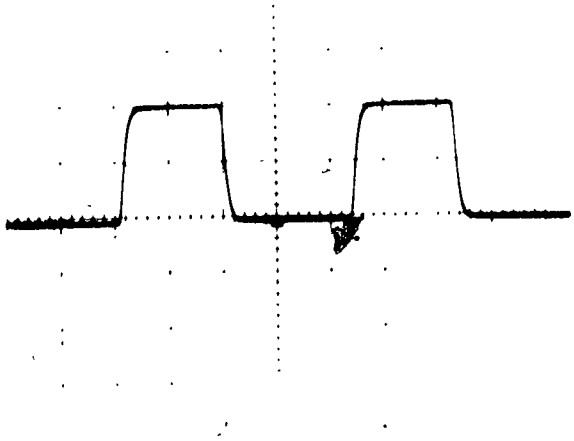

DAS 250 System Busy 2v and 1us/CM

```
7D01 TRIG   +1 0
     0000 0000 0000
     1010 0111 1010
     0101 0101 0100
     0000 0000 0000
     1110 1010 0000
     0101 0101 0101
     0001 0010 1000
     1111 1111 1111
     0101 0101 0110
     0010 1100 1001
     1111 1111 1111
     0101 0101 0111
     0100 0110 0010
     1111 1111 1111
     0101 0101 0111
     0101 1111 0000
     1111 1111 1111
     0101 0101 0100  TRIG
```

Digital Data

Figure 12 - Ramp Test 2

```
7D01 TRIG   +2 6
     1111 1111 1111
     0101 0101 0111
     0101 1011 1010
     1111 1111 1111
     0101 0101 0111
     0100 0001 1111
     1111 1111 1111
     0101 0101 0111
     0010 0111 0110
     1111 1111 1111
     0101 0101 0110
     0000 1100 0101
     1111 1111 1111
     0101 0101 0110
     0000 0000 0000
     1101 1010 1100
     0101 0101 0101
     0101 0101 0100  TRIG
```

```
7D01 TRIG   +4 2
     0101 0101 0101
     0000 0000 0000
     1001 0110 0001
     0101 0101 0100
     0000 0000 0000
     0101 0010 0101
     0101 0101 0100
     0000 0000 0000
     0001 0000 0010
     0101 0101 0100
     0000 0000 0000
     0000 1001 1111
     0101 0101 0100
     0000 0000 0000
     0100 1101 0001
     0101 0101 0100
     0000 0000 0000
     0101 0101 0100  TRIG
```

```
7D01 TRIG   +5 8
     0000 0000 0000
     1000 1101 1101
     0101 0101 0100
     0000 0000 0000
     1100 1111 1011
     0101 0101 0101
     0000 1000 0001
     1111 1111 1111
     0101 0101 0101
     0010 0010 0101
     1111 1111 1111
     0101 0101 0110
     0011 1100 0011
     1111 1111 1111
     0101 0101 0111
     0101 0101 0101
     1111 1111 1111
     0101 0101 0100  TRIG
```

```
7D01 TRIG   +7 4
     1111 1111 1111
     0101 0101 0111
     0110 0101 0111
     1111 1111 1111
     0101 0101 0111
     0100 1100 0100
     1111 1111 1111
     0101 0101 0111
     0011 0010 0001
     1111 1111 1111
     0101 0101 0111
     0001 0111 0010
     1111 1111 1111
     0101 0101 0110
     0000 0000 0000
     1111 0110 0010
     0101 0101 0101
     0101 0101 0100  TRIG
```

Digital Data

Digital Data

Figure 13 - Ramp Test #2

8. Square Wave Response

Figure 14 shows the response of the three transresistance amplifier types to a 10-kHz square wave input. These photos are filtered only by the oscilloscope, which has better than a megahertz response. In addition, the top set of pictures (Fig. 15) show the Burr Brown amplifier response to a 200 kHz square wave.

As expected, the higher the frequency response and slew rate of the amplifier, the better the response to the step function.

9. Picket Fence Test at 5 kHz

Figure 16 is a plot of the input and output data for Channel 1 with a f-kHz square wave applied to it. The sample rate was once per 15 μs or 66,000 sps/channel. The plots show that the 50-kHz filter is well settled by the third sample. This means that at the maximum sample rate of 20,000/sec in the flight system, the second sample after a step function will be a good sample. Figure 17 contains the photographs of the raw data.

10. Input Capacitance Test

Figures 18 and 19 show the affects of input capacitance on noise level. Only a few typical pictures were taken. The rest of the data are contained in Figure 20.

Two very important conclusions result from this test. First, conventional packaging should be considered for the flight system. Secondly, the cheaper national amplifier, which looks satisfactory from every other standpoint, does not look like a good choice from this test. The more expensive Burr Brown amplifier should be considered.

11. Ten Channel Static Test

Ten channels of the multiplexer were programmed. The sample rate was 20,000 sps on each channel. The analog channels were connected to the corresponding multiplexer channel. Because analog Channel 4 was broken, multiplexer Channel 4 was connected directly to the calibration voltage, which was adjusted to produce a 001010101011 pattern. The calibration voltage was also placed on the inputs of Channels 2, 5, 7, and 9. Channels 1, 3, 6, 8, and 10 were grounded.

The main point in this test is to examine the sample and hold amplifier with 10 channels flowing through the multiplexer. Figure 21 contains the test data and a comparison of calibration voltage calculated from Channel 4 output (1.667 V) and the current measured by Channels 2, 5, 7, and 9. The agreement is fairly good on three channels (0.7%), but poor on the fourth (2.38%). The severe offset in this channel is probably the source of error.

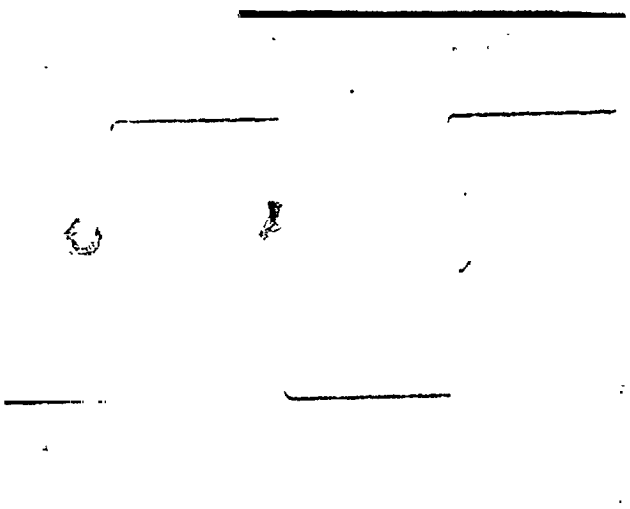

Calibration Voltage

National Output

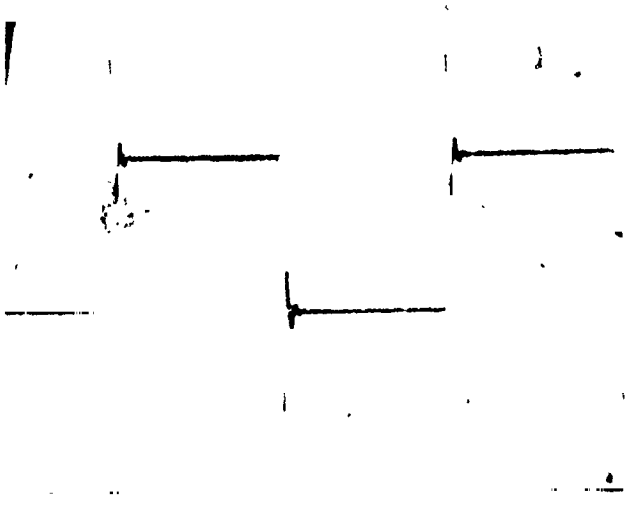

Datel Output

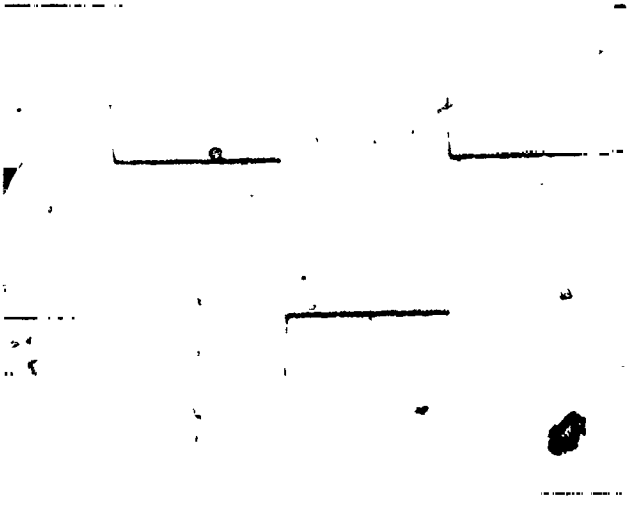

Burr Brown Output

Note - All Pictures are 2v and 20us/CM

Figure 14 - Input Amplifier Response to 10 KHz Squarewave

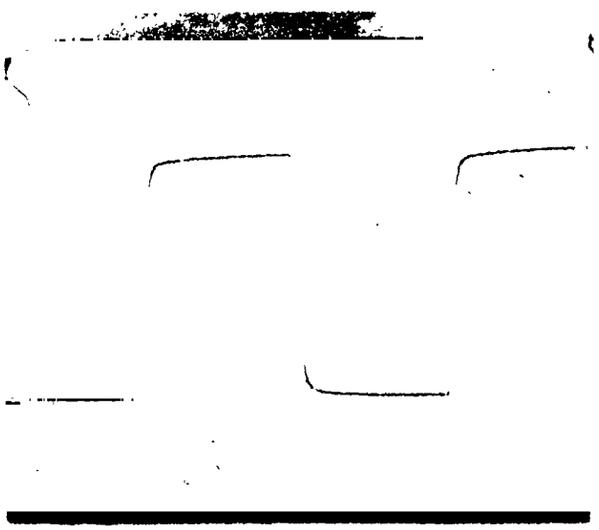

2v and 1us/CM
200 KHz Calibration Input to the
Burr Brown Amplifier

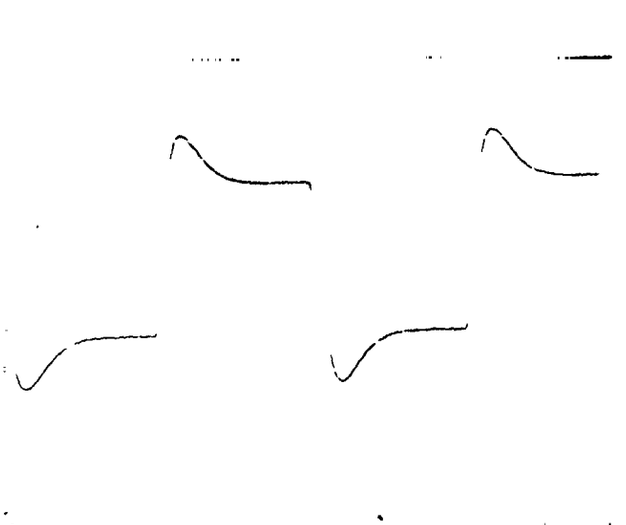

2v and 1us/CM
Burr Brown Amplifier Output with 200 KHz
Input

2v and 5us/CM Burr Brown Response to
10 KHz Squarewave

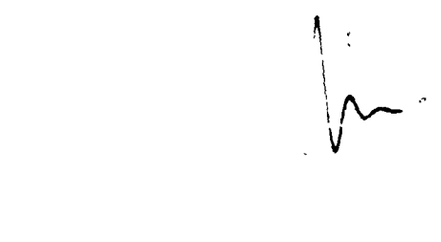

2v and 5us/CM Datel Response to
10 KHz Squarewave

Figure 15 - Burr Brown Response to 200 KHz and Expanded Pictures of the Datel and Burr Brown 10 KHz Outputs

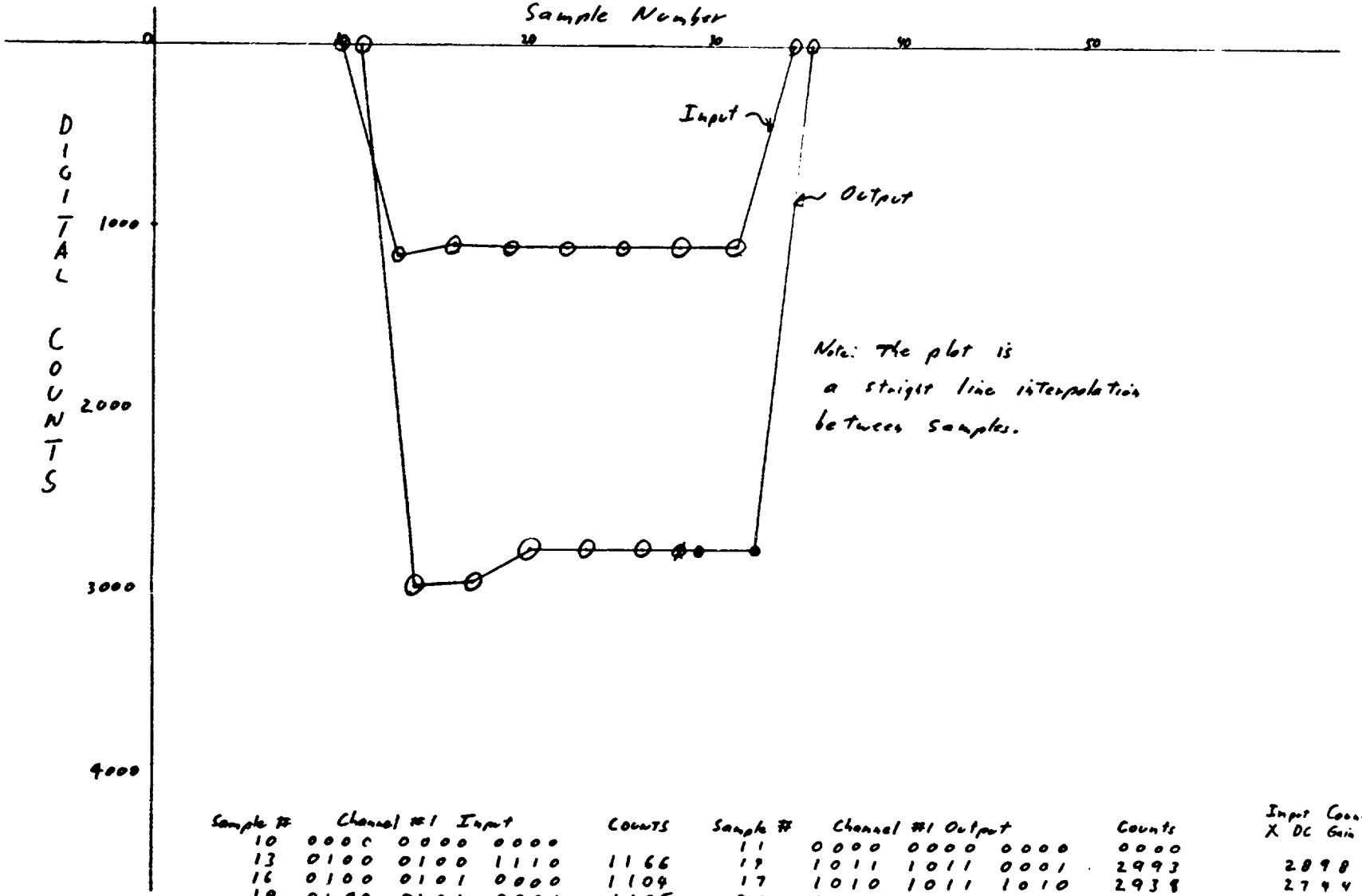

Sample #	Channel #1 Input			Counts	Sample #	Channel #1 Output			Counts	Input Counts X DC Gain Factor	% Difference
10	0000	0000	0000		11	0000	0000	0000	0000		
13	0100	0100	1110	1166	19	1011	1011	0001	2993	2898	3.28
16	0100	0101	0000	1104	17	1010	1011	1010	2938	2744	6.60
19	0100	0101	0001	1105	20	1010	1100	0101	2757	2747	.36
22	0100	0101	0001	1105	23	1010	1100	0101	2757	2747	.36
25	0100	0101	0001	1105	26	1010	1100	0101	2757	2747	.36
28	0100	0101	0001	1105	29	1010	1100	0110	2758	2747	.40
31	0100	0101	0001	1105	32	1010	1100	0110	2758	2747	.40
34	0000	0000	0000	0000	37	0000	0000	0000	0000		

Figure 16 - Channel 1 Response to 5 KHZ Square Wave

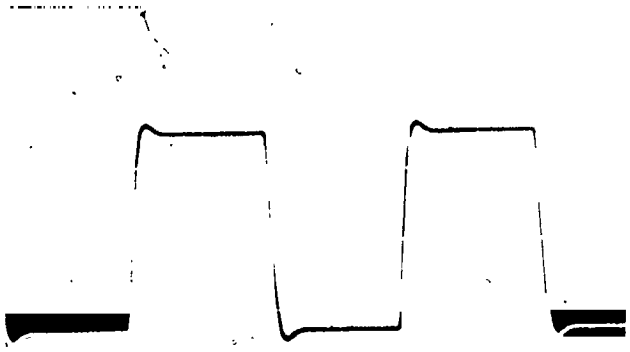

Channel 1 Output 5v and 50us/CM

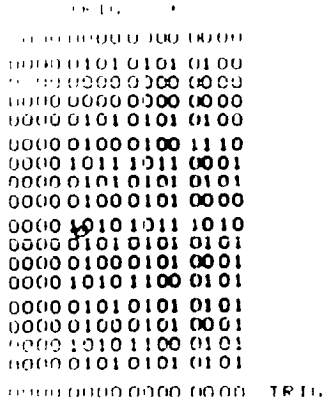

Digital Data

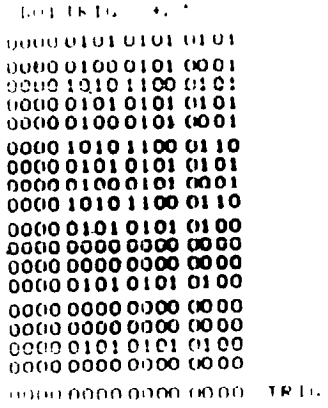

Digital Data

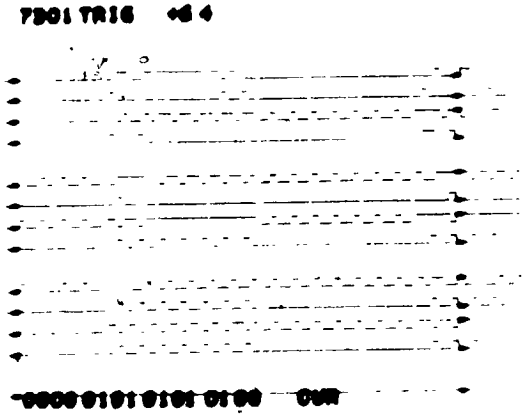

Digital Data

Figure 17 - Response of Channel 1 to a 5 KHz Squarewave

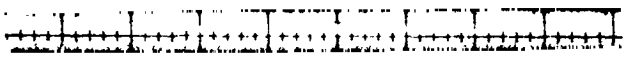

Channel 1 Output - Open Input 1mv and 200us per CM

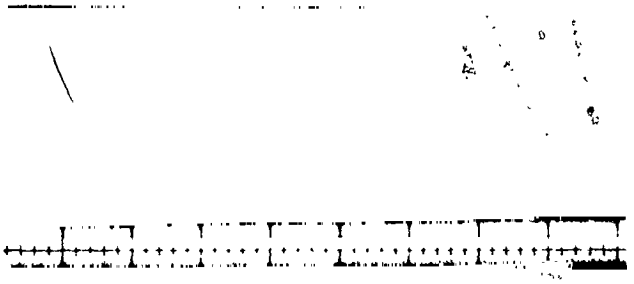

Channel 2 Output - Open Input 1mv and 200us per CM.

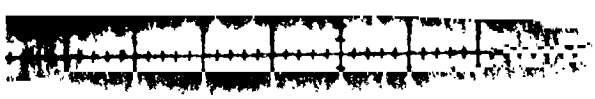

Channel 1 Output with 8' of RG58 on Input 10mv and 10ms per CM

Channel 2 Output with 8' of RG58 on Input 2mv and 1ms per CM

Figure 18 - Channel 1, 2, and 3 Output Noise Levels With Input Capacitance

Channel 1 Output With 4′ of RG58 on Input 2mv and 5us per CM

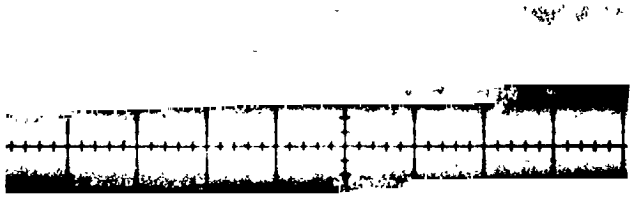

Channel 3 Output 8′ of RG58 on Input 2mv and 1ms per CM

Figure 19 - Channel 1 and 3 Noise Levels with Input Capacitance

TEST CONDITION	CHANNEL #	NOISE mv pk-pk
8' of RG58 on Input	1	35
	2	12
	3	12
330 pF glass capacitor access Input	1	30
	2	12
	3	12
4' of RG58 on Input	1	12
	2	4
	3	4
39 pF ceramic capacitor across Input	1	4
	2	2
	3	1.8
83 pF ceramic capacitor across Input	1	10
	2	3
	3	3
2' of RG58 across Input	1	12
	2	2
	3	2
	5	8
	6	2
	7	2
	8	1.7
	9	12
	10	7

Figure 20 - Channel 1, 2 and 3 Output Noise Levels As A Function of Input Capacitance

CHANNEL NUMBER	CHANNEL OUTPUT			COUNTS	ZERO COUNTS	AMPERES/ COUNT X 10^{-10}	INPUT CURRENT ua	CORRECTED COUNTS	CALCULATED CURRENT ua	% DIFFERENCE
1	0000	0000	0000	0000	-0002	4.935	1.0359			
2	0110	1010	0001	1697	+0020	4.987	.8293	1677	.8363	.84
3	0010	0101	0010	0594	+0594	4.9104	1.0258			
4	0010	1010	1011	683	NA	Cal Voltage 1.667V				
5	0110	1011	0010	1714	+0005	4.913	.8345	1709	.8396	.61
6	0000	0001	0101	0021	+0021	4.8915				
7	1010	0110	0100	2660	+0916	4.9291	.8406	1744	.8596	2.38
8	0000	0001	1110	0030	+0030	4.9476	1.0356			
9	0110	1011	0001	1713	+0003	4.9197	.8349	1710	.8412	.76
10	0000	0000	0000	0000	-0002	4.9147	1.0301			

Figure 21 - Ten Channel Test

12. Major Overall Test Conclusion

1) The electronics portion of the imaging system will provide a dc to 10,000 Hz bandwidth that is flat and contributes no more than 0.4% of full-scale uncertainty to the measurement;

2) Conventional packaging is adequate for the transresistance amplifier design;

3) Because of the sensitivity of operational amplifier voltage noise to input capacitance, the Burr Brown amplifier should be slected for the flight system.

B. DETECTOR ARRAY TESTS

Three tests were performed which required two changes to the electronics breadboard described in the previous section to better simulate the flight system. First, it was recognized that higher gains would be required in the flight system so the feedback resistor for Channels 2, 4, and 8 were changed to 5.1487 MΩ, 5.040 MΩ, and 5.118 MΩ, respectively. With a nominal gain of 4 in the second stage amplifier, the effective feedback resistance was on the order of 20 MΩ. This resulted in a full-scale measurement current for these channels of about 0.5 μamp.

The second major change was that rather than simulating currents, the measurement current was provided by an indium antimonide sensor array mounted in a LN_2 dewar. Each detector was 0.002 in. on a side. The infrared for the test was provided by a calibrated blackbody. Figure 22 is a schematic of the optical breadboard. It is noted that this particular optical arrangement provided four times the energy density, at a given temperature, that will be provided by the flight system. This was done to exercise the electronics over more of the measurement range because the blackbody could only produce a maximum temperature of 1273°K. The three channels with the 5 MΩ feedback resistor were scaled to maximum temperature range of 1900°K. Of course, the data were corrected for this difference before any assessment of flight system performance.

1. Sensor Paralleling

Because the flight system will parallel three detectors into each amplifier channel, nine of the breadboard detectors were connected in sets of three into Channels 5, 6, and 7. Four sets of data were taken to evaluate the effects of this arrangement. The DAS 250 output of each channel with only one detector connected and without an infrared signal provided the baseline reading. Then

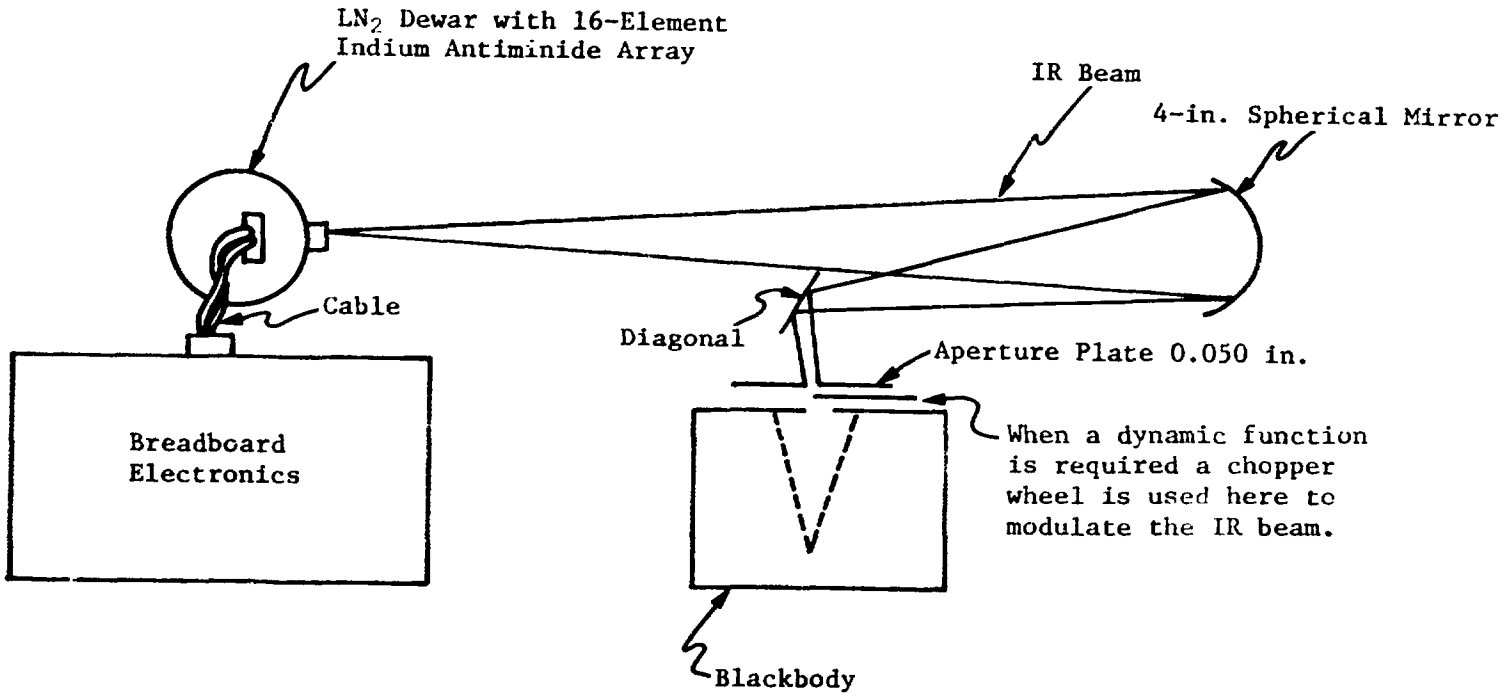

Figure 22 Optical Schematic for Array Tests

the two additional detectors were added, and, again, the DAS 250 output recorded. The third test condition was back to the non-paralleled configuration but with dc IR energy on the array. The fourth condition then was with IR and paralleling. The compliments of the raw data and the deltas produced in each configuration are shown in Figure 23. The data show a loading effect of three counts without an IR signal. This will not be a problem in the flight system and can be accounted for by the calibration procedure. When paralleling was done though with IR falling, fust on one detector of each set of three, a substantial delta of 25 counts accrued. This was attributed to "optical crosstalk" in which unwanted IR energy falls on the other detectors in the array. In the flight system, this effect will be negligible due to the much greater physical separation of the paralleled detectors.

2. Optical Crosstalk

To quantify optical crosstalk a special test was run. Figure 24 shows the test in which the image of the 0.050-in. aperture was focused on the upper part of the array containing the detectors that were paralleled with Channels 5, 6, and 7. The exact location of the image was not known, but none of the direct image fell on the "primary" detectors 1 through 10 at the bottom of the array. An examination of the data in Figure 24 shows that Channels 1, 2, 3, 4, 8, and 9, which did not have paralleled detectors and which should not have had IR on them, experienced a delta count change from 1 to 12 when the IR source was turned on. The conclusion is that indirect IR energy was reaching these detectors.

With all channels scaled to constant gain (i.e., Channels 2, 4, and 8 outputs divided by 4) and percentages expressed as a percent of energy density, the crosstalk is seen to be from 0.7 to 3%. As a source of measurement error, this is the greatest single source of error found in the testing and extreme attention must be paid to this element in the flight system design.

3. Infrared Pulse Response

The question answered by this test is, "Does the addition of the detector to the measurement electronics produce a change in the dynamic response of the measurement channel?" Figure 25 shows the test setup in which a chopper wheel was installed in the blackbody and rotated to move an image across a single detector in less than 30 μs. This is a rate almost double that of the fastest pass in the flight system.

PARALLELING OF DETECTORS

Channel Number	No IR and Not Paralleled	No IR but Paralleled		With IR Not Paralleled	IR and Paralleled	
		Absolute	Delta		Absolute	Delta
5				3580	3555	25
6	4079	4079	3	3507	3482	25
7	3160*	3157	3	2683	2654	29

Noise increases 50 to 100% after paralleling.

*The bias on Channel 7 was not adjusted for this test.

Figure 23 Paralleling of Detectors

DETECTOR ARRAY OPTICAL CROSS TALK

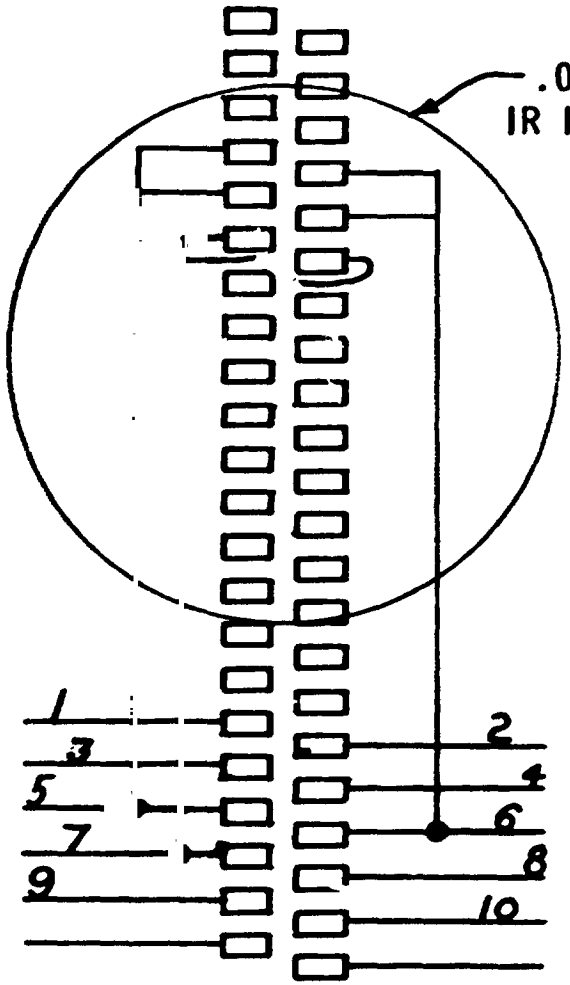

Channel	No IR	With IR	CROSS TALK Counts	%
5	4	274		
6	20	292		
7	20	257		
1	3	7	4	3
2	12	24	12	2.2
3	11	14	3	2.2
4	6	17	11	2.0
8	7	15	8	1.5
9	14	15	1	.7

Figure 24 - Detector Array Optical Cross Talk

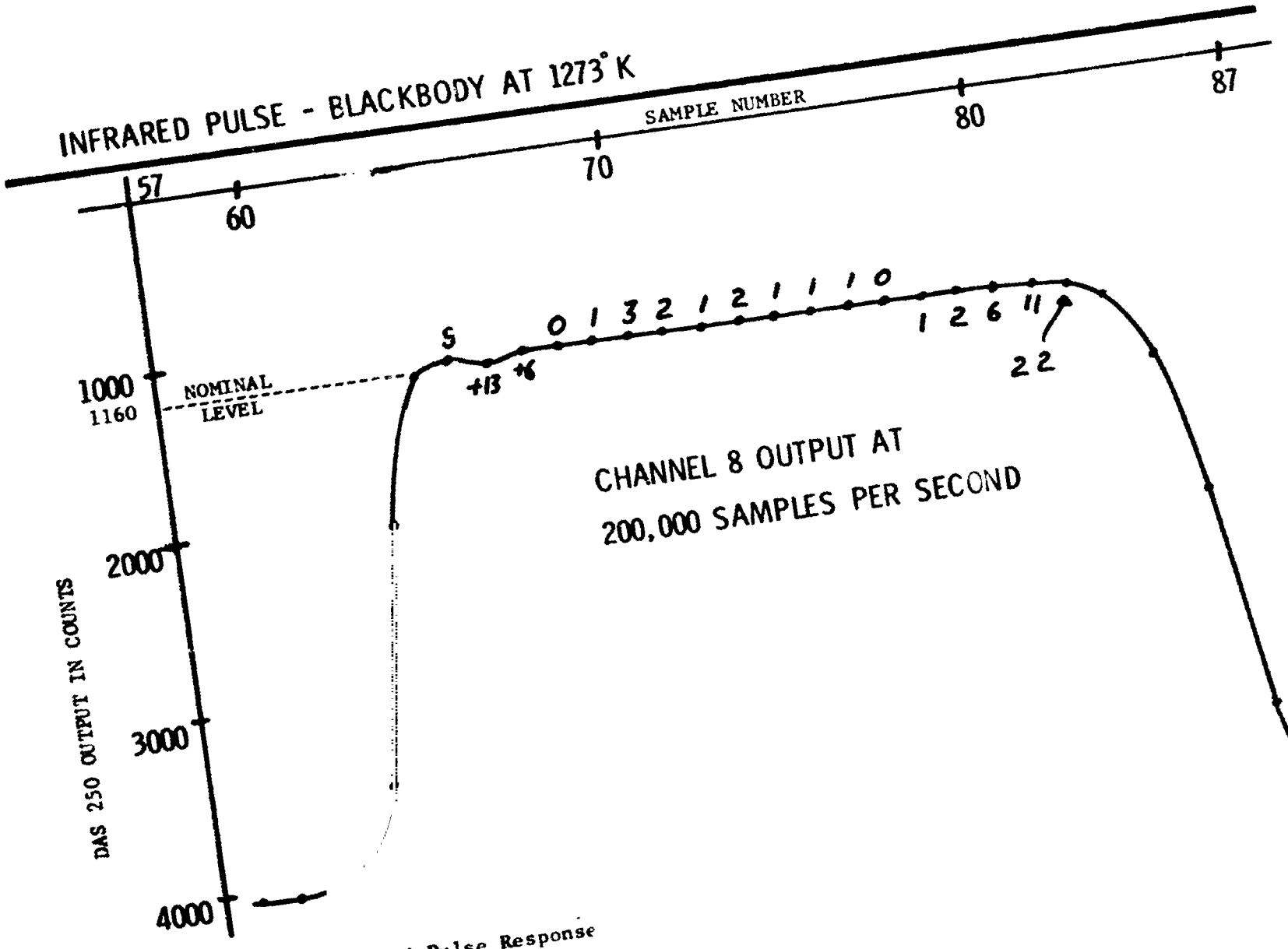

Figure 25 - Infrared Pulse Response

An examination of the pulse plot in Figure 25 clearly shows that all transient and frequency dependent effects are gone within 35 μs after the wave has peaked. In other works, the detector and the electronics are responding exactly as if the signal were dc at this point. The conclusion from this test is that the flight system can be calibrated from end to end at dc with the result that returned flight data will not contain greater error than the dc calibration within one sample period (50 μs) after a step function in the IR flux. The sample rate for this test was selected at 200,000 sps to provide a fine grained look at the ramp function, the overshoot of the amplifier response and the settling time on the top of the square wave.

4. Blackbody Response

Array data were taken on all channels as a function of blackbody temperature. Channel 8 data are plotted in Figure 26, 27, and 28. Figure 26 is a plot of the raw data from 600 to 1200°K with the enhansed flux density as previously described. Temperature resolution is also shown. As a point of reference, one count will resolve 0.25°K in this test. Figure 27 shows the channel output corrected to show the flux density that would be experienced in flight. The temperature resolution in this case, is 1°K per count at 1000°K.

For a further comparison the measurement response and resolution as predicted in the Task 1 study and as measured in this task are plotted in Figure 28. As previously stated, the magnitude of the detector current was overestimated in Task 1. That clearly shows in Figure 28, but with the amplifier gain increased, the test data show that the predicted resolution is obtainable.

5. Detector Responsivity

The responsivity of the detector on Channel 8 was checked to make sure that it is similar to that which can be expected in the flight system array. That was found to be the case. The following table represents the responsivity as a function of temperature for Channel 8.

Temperature	Nano-Amperes	Nano-Watts	Responsivity (Amp/Watt)
613	0.34	0.25	1.37
716	1.4	1.1	1.3
821	4.3	3.2	1.35
930	10	7.7	1.315
1035	20	1.5	1.36
1143	36.7	2.7	1.36
1251	59	4.4	1.35

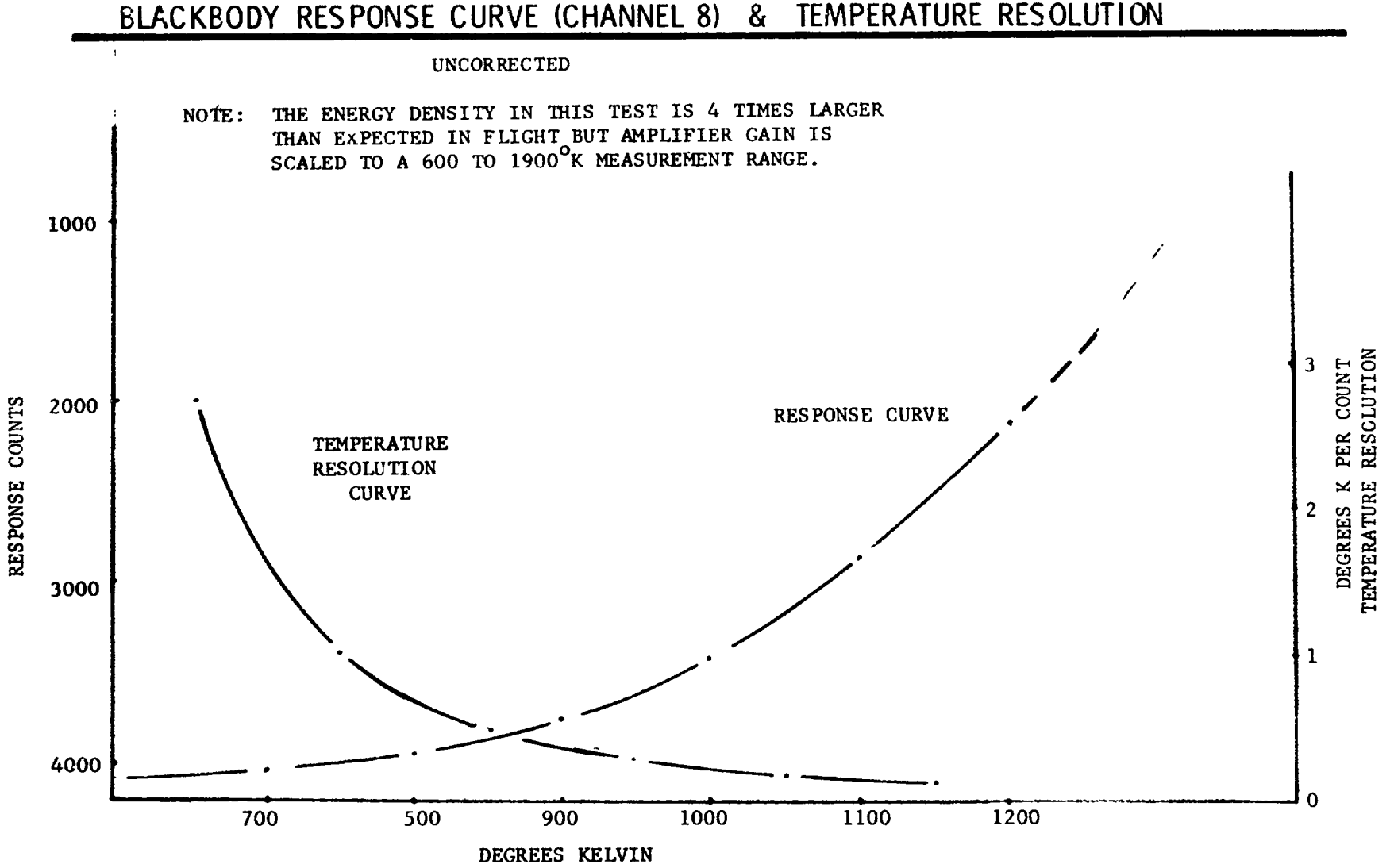

Figure 26 - Uncorrected Channel 8 Blackbody Response and Resolution

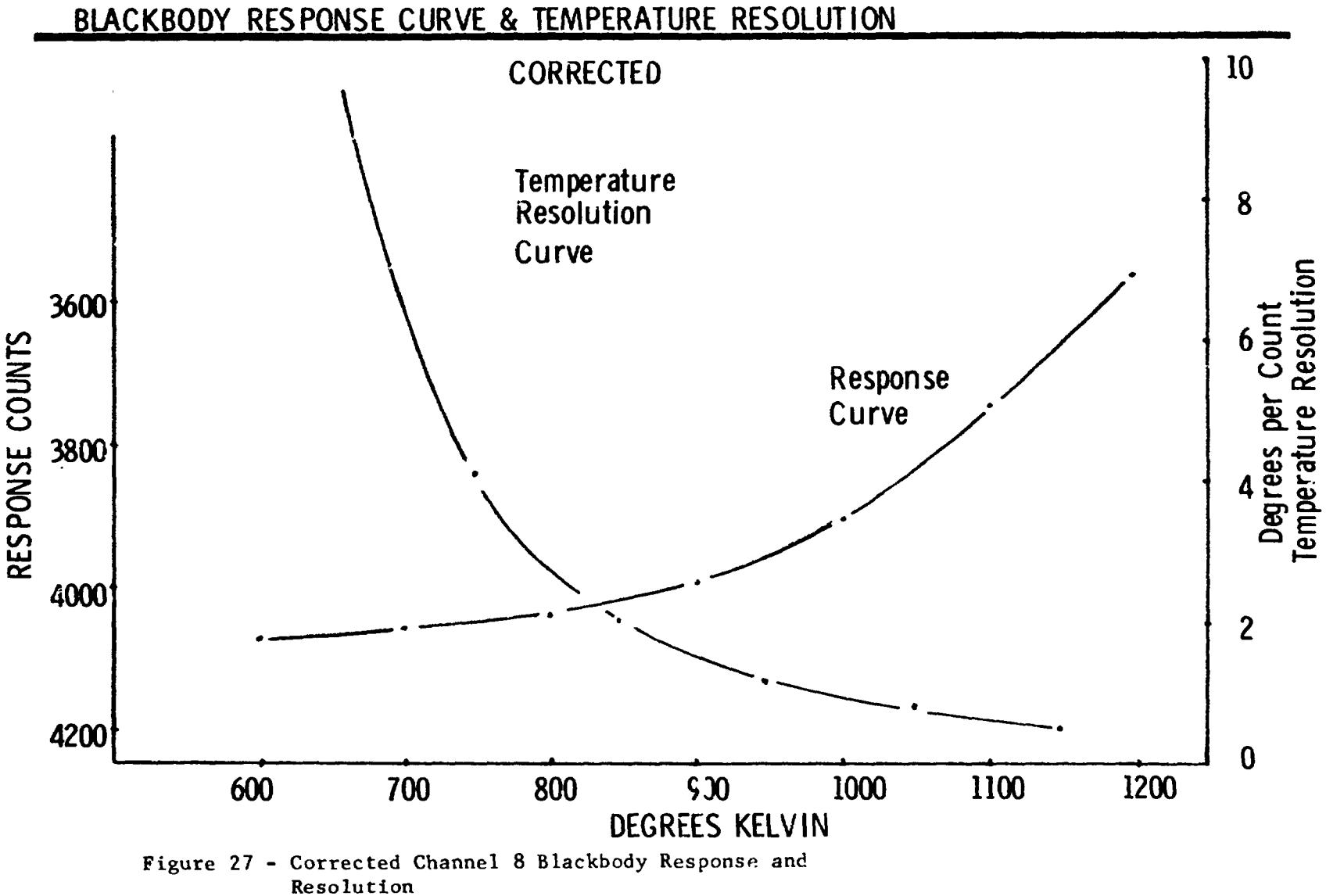

Figure 27 - Corrected Channel 8 Blackbody Response and Resolution

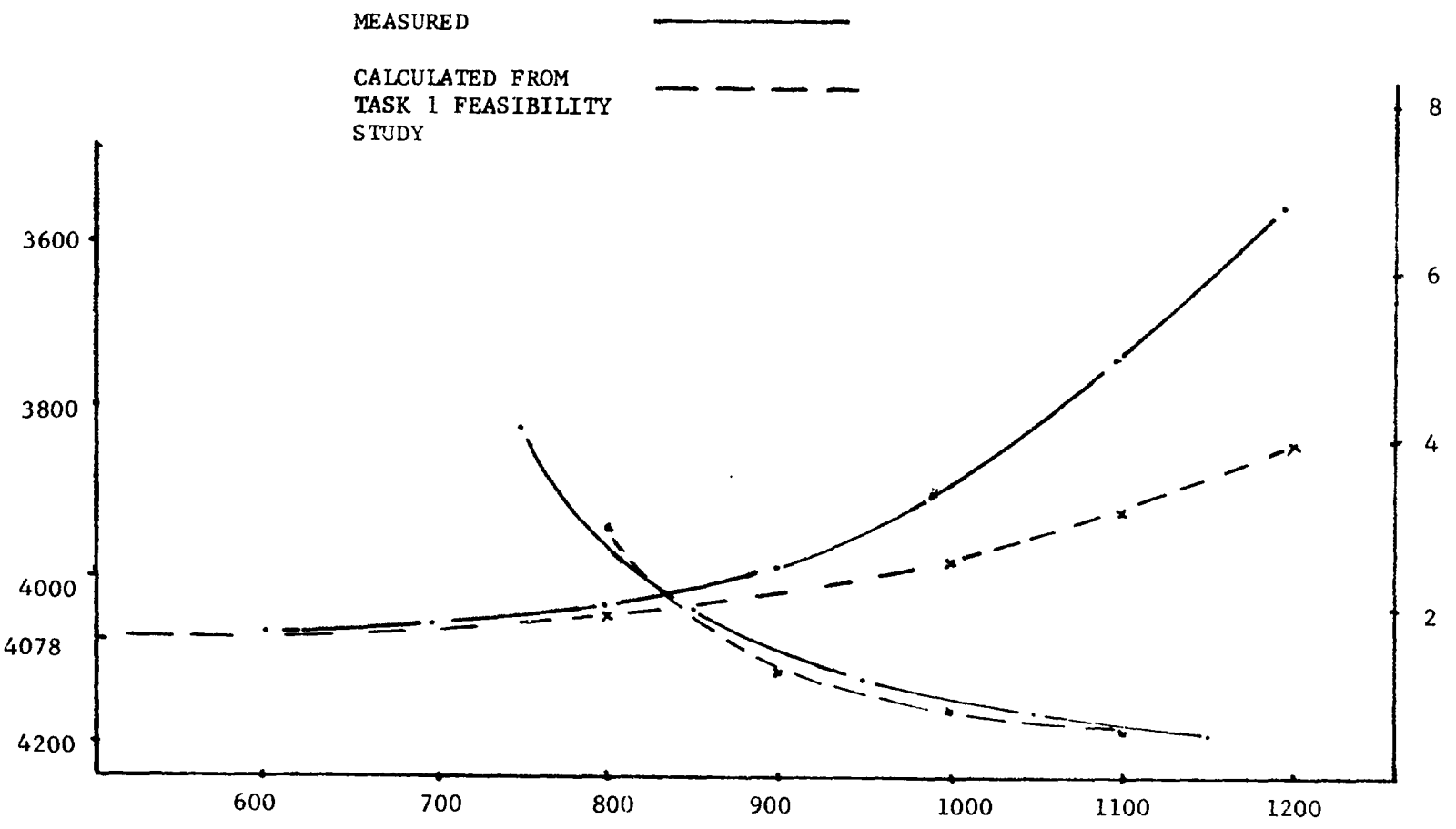

Figure 28 - Channel 8 measured response compared to Task 1 predictions

6. Conclusion

No better summary is possible than to assess the measurement error expected from all the sources tested. Figure 29 is a table of error contributed by each source. The RSS of these errors is four counts. This represents an uncertainty of ±4°K at 1000°K or an absolute measurement accuracy of 0.4% of reading. At higher temperatures the readings are more accurate and at lower temperatures less accurate. To go back to the original criteria of 2.5% of reading as the goal, the lowest temperature to meet the criteria would be around 720°K. This is in fairly good agreement with the 2.5% of 700°K design goal described in the Task i report. It should be recognized that some error sources are not represented in the error summary such as the optical crosstalk item treated previously. However, no allowance has been made for an improvement in accuracy by use of end to end IR calibrations. In summary, the final conclusion is that high-quality measurements can be made to the accuracies required.

PARAMETER	MEASUREMENT UNCERTAINTY IN COUNTS		TEMPERATURE UNCERTAINTY °K In 900 to 1000°K Region
Noise	1		1
DC Gain	3		3
AC Gain	2		2
DAS250	2		2
RSS ERROR	4 Counts	RSS ERROR	4°K

Figure 29 - Measurement Error Summary

II. ACQUISITION SYSTEM ANALYSIS AND TEST

Three distinctly different topics are treated in the following sections of this chapter.

Section A is an analysis that was generated before the reticle tests. Its purpose was to establish the extent to which the tracking system electronics needed to be simulated in the breadboard. In addition, the nature of the generated waveforms by the test reticle was examined and a number of ways of processing them were defined. This analysis provided a basis for the selection of a candidate reticle system.

Section B is an analysis of the amplifier response necessary to provide accurate reproductions of reticle signal transitions for a rotation rate of 20 to 30 rps. The analysis concludes that the 25-kHz bandwidth is acceptable.

Section C contains pictures of the test reticle output, an analysis of those pictures, and a block diagram of the candidate electronics for processing the reticle signals. Azimuth error is discussed, and some of the remaining considerations in the tracking system electronics are listed.

A. ANALYSIS OF RETICLE WAVEFORMS AND METHODS OF ELECTRONIC PROCESSING

Figure 30 shows, in simplified form, the clock track signal and the IR sensor signal waveforms. The feature of main concern is the rise time of each waveform. It is clear that the rise times shown (57 μs for the clock track and 250 μs for the Shuttle image) are extremely slow relative to TTL switching speeds and that conventional TTL logic is more than adequate for this signal processing electronics.

Two basic ways of processing the reticle signals are possible:

1) Use only the clock track for counting;

2) Use an external clock and count between clock pulses.

Rise time calculation of sync and clock pulse

Detector Beam Diameter = 1/32"

The clock/sync track covers 1/32" @ 50 RPS in:

$$\frac{1/32"}{(3\frac{1}{2}") \times 50 \text{ RPS}} = .00057 \text{ sec}$$

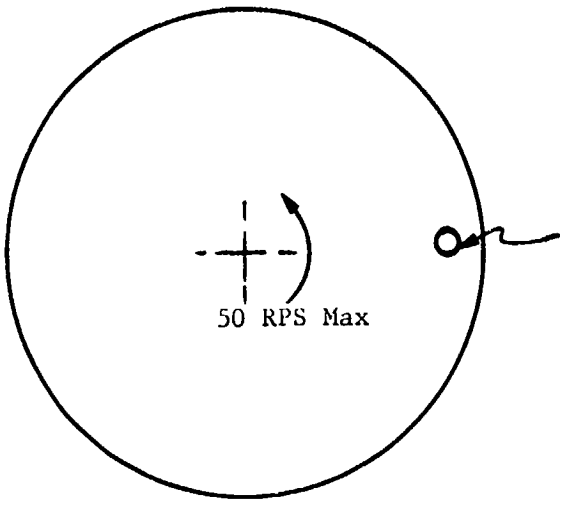

Reticle Diameter 3½" (Clock Track)

Sensor Beam Diameter 1/32"

The reticle moves 1/32" in 57 μs

Clock Track - The clock track is a 50% duty cycle clock. A cycle is:

$$\frac{1}{60}\left(\frac{1}{50}\right) = \frac{1}{3000} = 333 \text{ μs}$$

So the clock track output will look like:

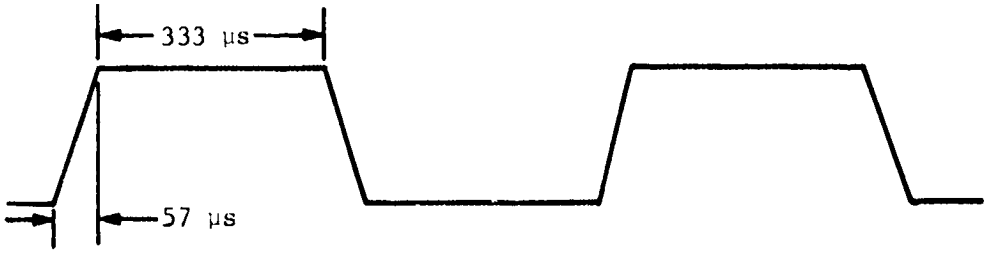

Shuttle Image Sensor Output at "Null"

(Without Frequency Modulation)

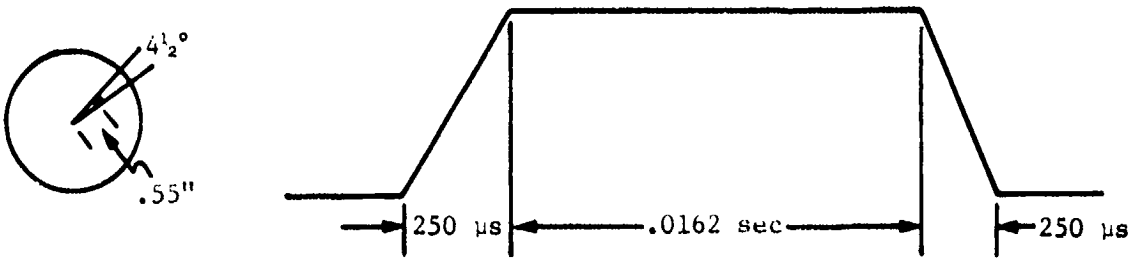

Figure 30 Reticle Waveforms

Now each of these two basic approaches can be implemented with one of three features:

1) Discrete threshold detection;

2) Programmable discrete threshold detection;

3) Analog-to-digital conversion of one or more of the output functions and threshold detection by "digital word mask."

Analysis of these various elements leads to the conclusion that although there are many different system configurations that will do this job, all of these proposed system configurations employ similar analog signal processing. Any apparent difference in signal processing lies in the method of converting the analog signals to digital signals. All of the proposed digital processing systems are conventional and easily within the state of the art. Some conclusions are:

1) There are no principles that need proving or techniques to be developed relative to the digital processing;

2) Only a specific method of digital processing must be selected for the flight system;

3) Only tests to establish the exact nature of the "analog" signals from the reticle are required in the breadboard.

B. RETICLE IR SENSOR AMPLIFIER BANDWIDTH ANALYSIS

All the IR energy passing through the tracking system reticle is focused on a single indium antimonide detector. When the Shuttle image is present on the reticle it is turned on and off or modulated by the rotating clear and opaque portion of the reticle. The purpose of this analysis is to determine the amplifier bandwidth required for the detector signal without "rounding it off" or in essence removing information from the wave forms.

The highest frequencies are generated when the Shuttle image is modulated by the outer reticle band that contains seven transparent areas and six opaque areas on one half of the reticle. With the reticle spinning at 30 rps, half of the reticle produces a periodic trapazoid function with a fundamental sine wave component of 30x7 or 210 Hz. The other half of the reticle is completely opaque and produces no output. To simplify this analysis, an assumption is made that the 210-Hz trapazoid function is continuous around the complete reticle. This will allow a standard Fourier series representation of the wave.

Using the additional criteria that the Shuttle image size should be exactly one half the width of a black or transparent area, the following IR flux function will fall on the detector:

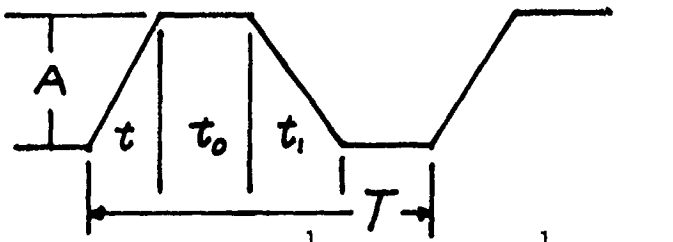

$$\text{The Period } T = \frac{1}{\text{Reticle RPS}} \cdot \frac{1}{\text{Modulation Zones}}$$

$$T = \frac{1}{30} \cdot \frac{1}{13} = .00256 \text{ sec}$$

The amplitude of each sine wave component for this waveform is:

$$C_n = 2\, A_{AVG} \frac{\sin \frac{n\, t_1}{T}}{\frac{n\, t_1}{T}} \cdot \frac{\sin \frac{n\,(t_1 + t_0)}{T}}{\frac{n\,(t_1 + t_0)}{T}}$$

$$t_1 = t_0 = \tfrac{1}{4}\, T$$

$$C_n = 2\, A_{AVG} \frac{\sin \frac{n}{4}}{\frac{n}{4}} \cdot \frac{\sin \frac{n}{2}}{\frac{n}{4}}$$

$$C_n = A_{AVG} \frac{\sin_{0.79n}}{0.39n} \cdot \frac{\sin_{1.5700}}{0.79n}$$

$$C_n = A_{AVG} \frac{\left(\sin_{0.79n}\right)\left(\sin_{1.57n}\right)}{0.31n^2} = A_{AVG} \frac{0.71}{0.31n^2}$$

$$C_n = \frac{2.29}{n^2}$$

The following table lists the sine wave amplitudes at selected frequencies.

n	Fraction of $A_{AVERAGE}$	Frequency, Hz
1	2.29	390
3	0.25	1,170
5	0.09	1,950
7	0.04	2,730
9	0.03	3,510
10	0.02	4,290
13	0.014	5,070
15	0.010	5,850
17	0.008	6,630
19	0.006	7,410
37	0.002	14,430
73	0.0004	28,470
145	0.0001	56,550
289	0.00003	112,710

A reasonable method of selecting the passband is to determine the highest frequency necessary to select the sine wave component whose amplitude is equal to the average value of the waveform divided by the signal-to-noise ratio. From the Task 1 report the S/N ratios range from 4580 to 1900 depending on the range and the temperature of the Shuttle.

The average signal to noise ratio is 2806, so the lowest signal of significance is $\frac{A_{AVERAGE}}{2806} = 0.0004\ A_{AVERAGE}$. This is approximately equal to the $0.0004\ A_{AVERAGE}$ listed for the 28,470 Hz component in the Fourier series.

This means that for the average S/N of 2806, a 25 kHz amplifier bandwidth is appropriate. It is noted that this bandwidth is not best for the YF12 pass, which produces a S/N ratio of only 200. Less bandwidth would improve the overall tracking of the YF12 but unless it becomes a requirement to design for the YF12 pass, it is recommended that the amplifier bandpass be kept at 25 kHz.

C. RETICLE TESTING AND SIGNAL PROCESSING

Figure 31 contains pictures of the simulated Shuttle image in transition from Zone 2 to Zone 3. A key question is the best method for waveform discrimination for zone detection. It is apparent from the waveforms that the cleanest transition always occurs in the two outside pulses. A simple clean transition in pulse width simply moves from the bottom of one side of the pulse to the top. A simple way to detect this is to slice the waveform in the middle and make a transit time measurement. When the step function crosses the slicing threshold a discrete change will take place. Now, if there is some tendency for the change not to be discrete, then hysteresis can be added to the slicing circuit.

If the mask position readings for Zone 2 is subtracted from the reading for Zone 3, it is seen that the transition occurred with an image movement of 0.070 in. In the reticle test configuration the distance from the Shuttle mask to the objective is 10 3/4 in. and the distance from the objective to reticle is 12 5/16 in. Therefore, a mask movement of 0.070 in. produces an image movement of

$$\frac{12\ \frac{5}{16}}{10\ \frac{3}{4}}\ (0.070) = 0.080 \text{ in.}$$

In the waveform slicing circuit, it is easily possible to slice with no more uncertainty than 1 part in 70. This means that the zone "transition" can be defined to 0.001 in. This estrapolates to an uncertainty in the Shuttle radius calculation of only 46 arc sec. This is only a small portion of the radius error due to the band dimension of 7 arc min and, therefore, is of no concern.

Figure 32 is a block diagram of the reticle signal processing electronics and Figure 33 is a photograph of the test setup. Two key thoughts are necessary to understand the diagram. The first is that both the Shuttle image phase angle and the Shuttle image radius are measured by counting time. The concept of counting a frequency to determine the Shuttle image radius has been eliminated from this system concept. The second element to be understood is that a very high resolution clock track has been replaced by a low resolution clock track and a vernier electronic clock that counts time between pulses from the clock track. The reason for this change is that it will increase the probability of being able to use a conventional optical sensor in the flight system design. It should also be noted that a dynamic, programmable threshold detector is shown for converting the Shuttle image signal to a logic function. This has been added to handle change in the Shuttle image intensity and to allow for some background signal.

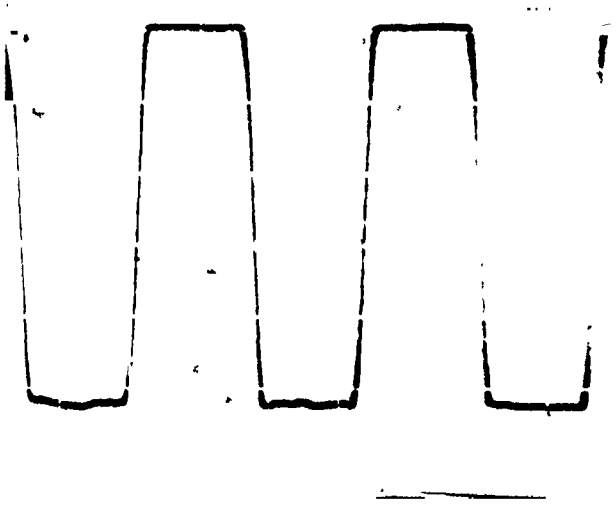

Zone 2 50mv/CM
2ms/CM
Mask Position .795 in.

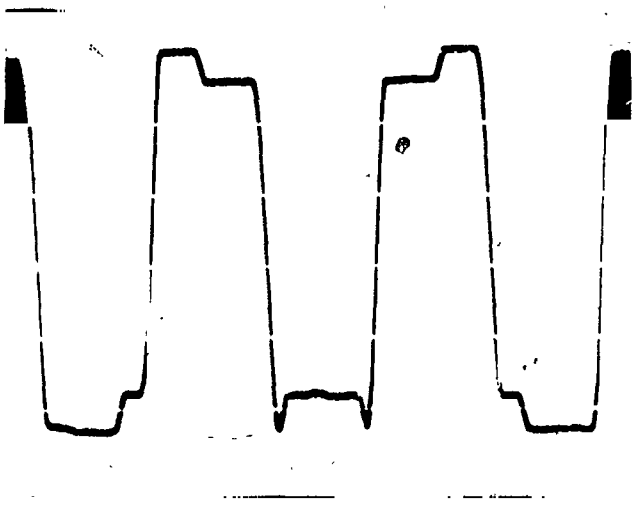

Mask Position .785 in.

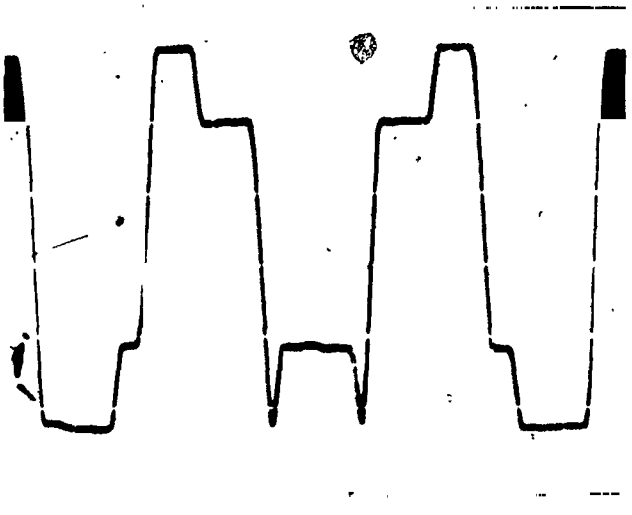

Mask Position .775 in.

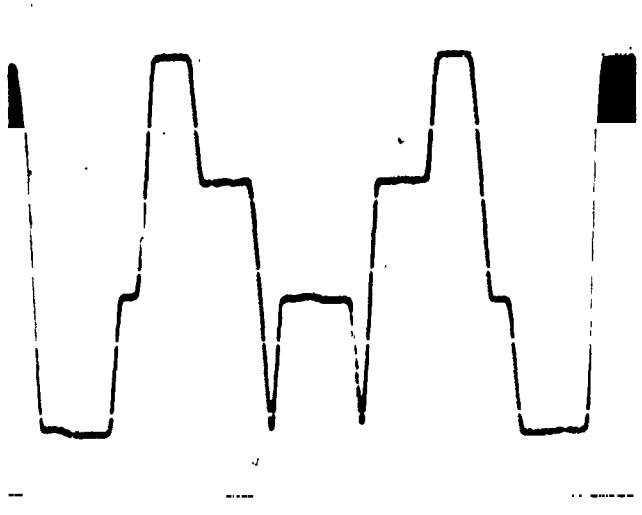

Mask Position .765 in.

Figure 31 - Image Transition from Zone 2 to .

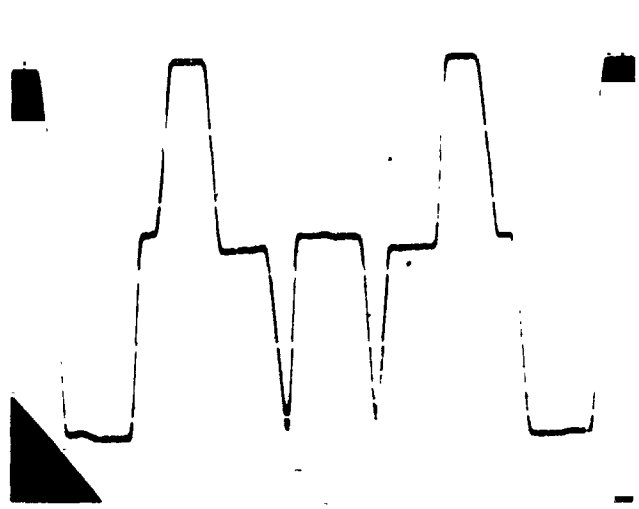

Mask Position .755 in.

Mask Position .745 in.

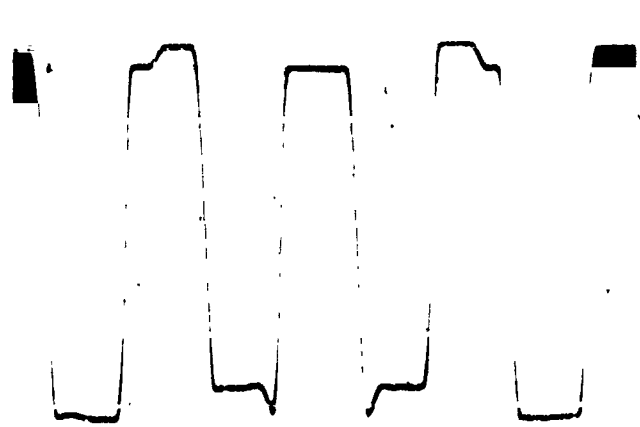

Mask Position .735 in.

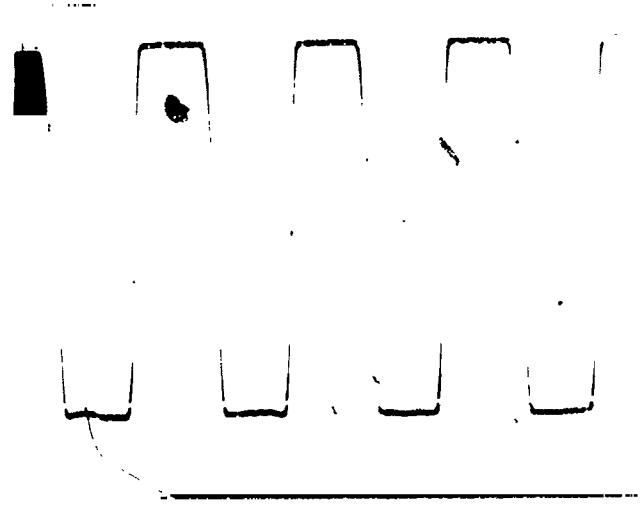

Zone 3 Mask Position .725 in.

Figure 31 - Continued

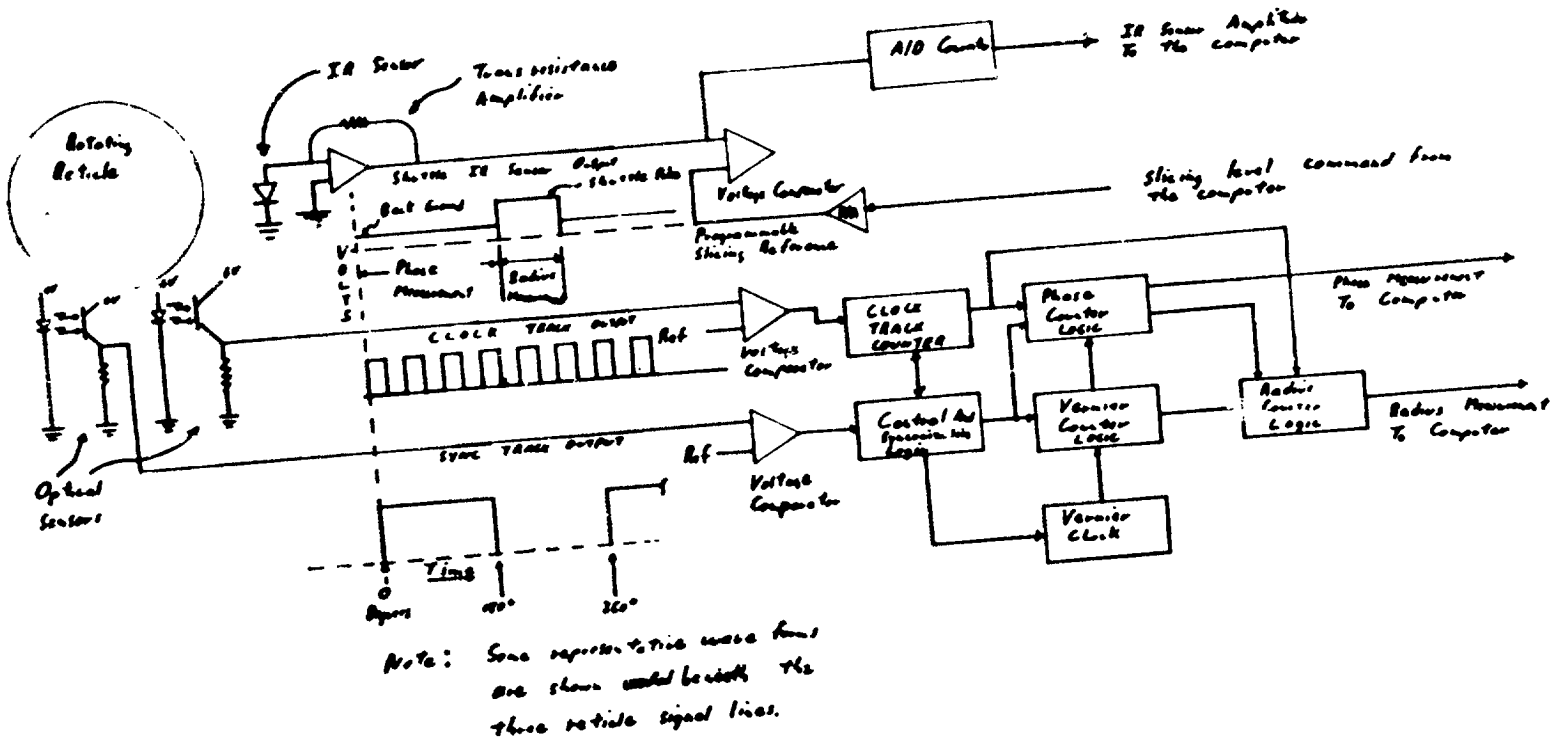

Figure 32 - Block Diagram - Reticle Signal Processing

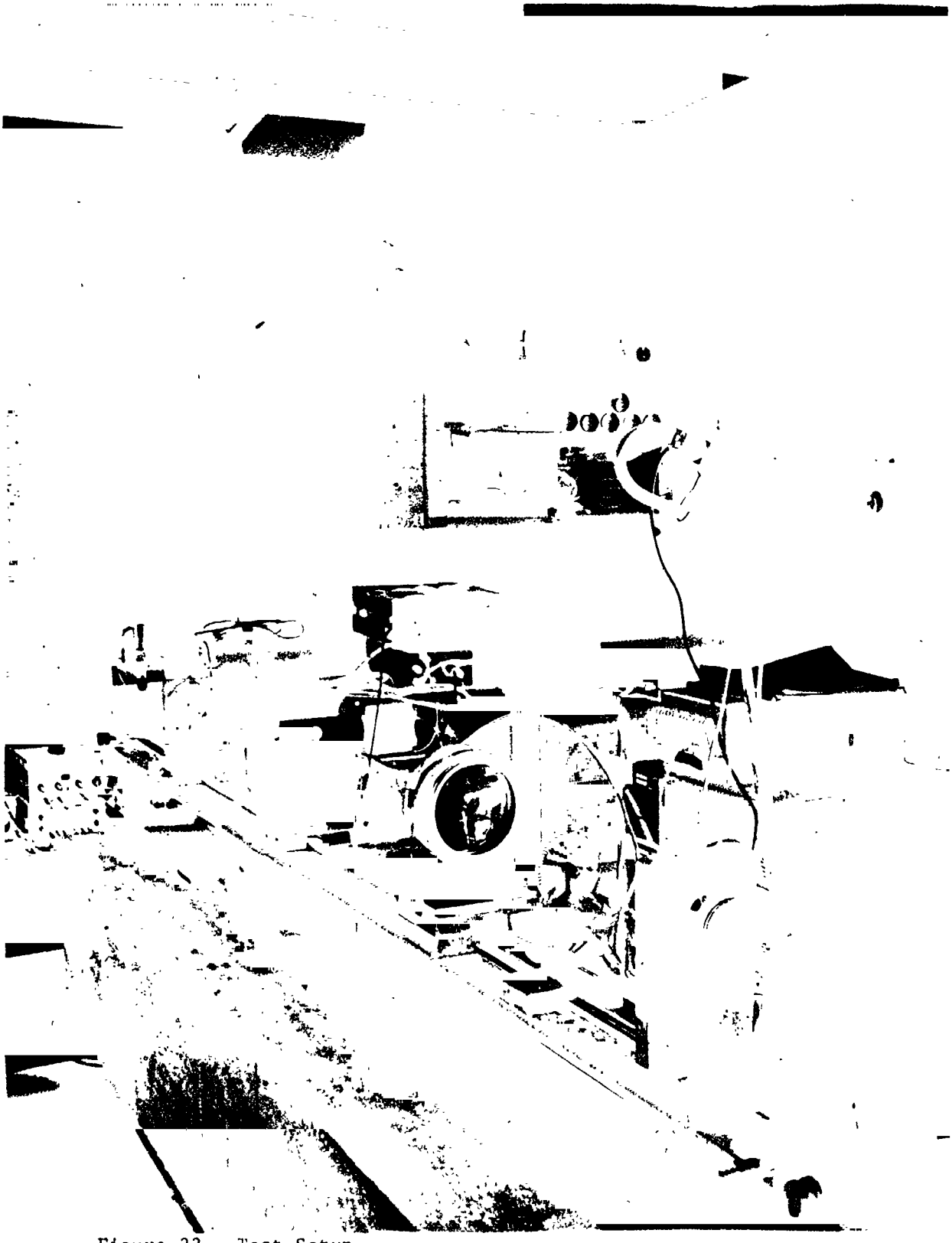

Figure 33 - Test Setup

It is apparent that the baseline reticle is not optimized for the type of electronic processing presented here. Figure 34 presents a reticle concept that will provide proportional information to the control computer for the radius measurement as well as the angular measurement.

The equation for the curve is $r = 0.4 \frac{\theta}{180}$ where r and θ are as shown in Figure 34 and 0.4 in. is the radius of the flight reticle. All servoanalyses have been based on tracking set point being at a radius of 0.027 in. At this radius, the clear gap in the reticle will be 0.0057 in. The Shuttle image size is about 0.0022 in. Even with blur contributed by the optics, the Shuttle image will be smaller than the gap in the reticle. The conclusion reached is that at the tracking point the Shuttle signal will still be of full amplitude. The concern is that as the Shuttle image approaches the axis of the reticle, at some point the clear gap in the reticle will be smaller than the blur circle and the signal will be amplitude modulated. This, of course, would affect the slicing level and the precision of the Shuttle position measurement.

Conclusions -The radial uncertainty in image position based on test data will not exceed 46 arc sec assuming an ability to slice the waveform to 1 part in 70.

The circumferential uncertainty in image position is 6 arc min at the edge of the reticle but is reduced by a factor of 183 at the tracking set point or 2 arc sec, again based on an ability to slice the Shuttle image waveform to 1 part in 70.

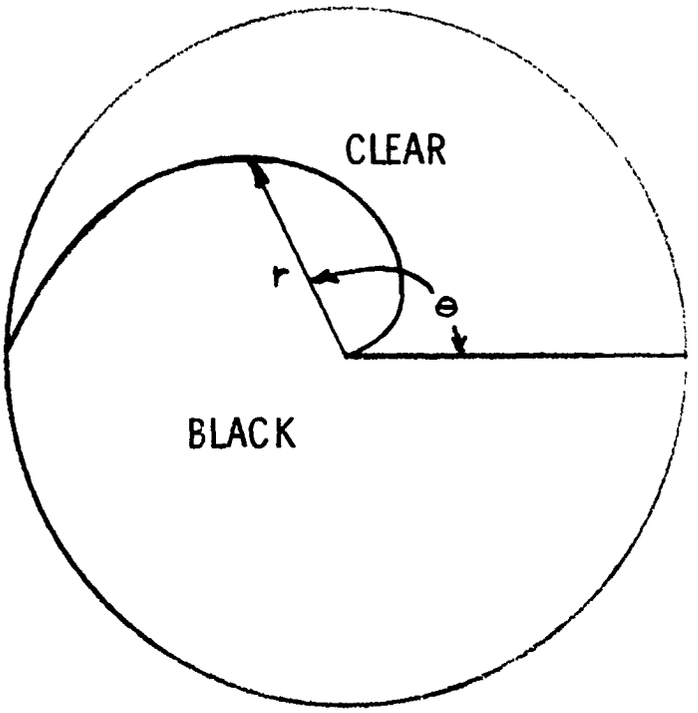

NOTE: Clock and Sync Tracks are not shown.

Figure 34 - Potential Reticle Redesign